RIGA TECHNICAL UNIVERSITY

Kārlis Gulbis

DEVELOPMENT OF THE SYNCHRONOUS RELUCTANCE MOTOR FOR APPLICATION IN PUBLIC TRANSPORT

Summary of the Doctoral Thesis

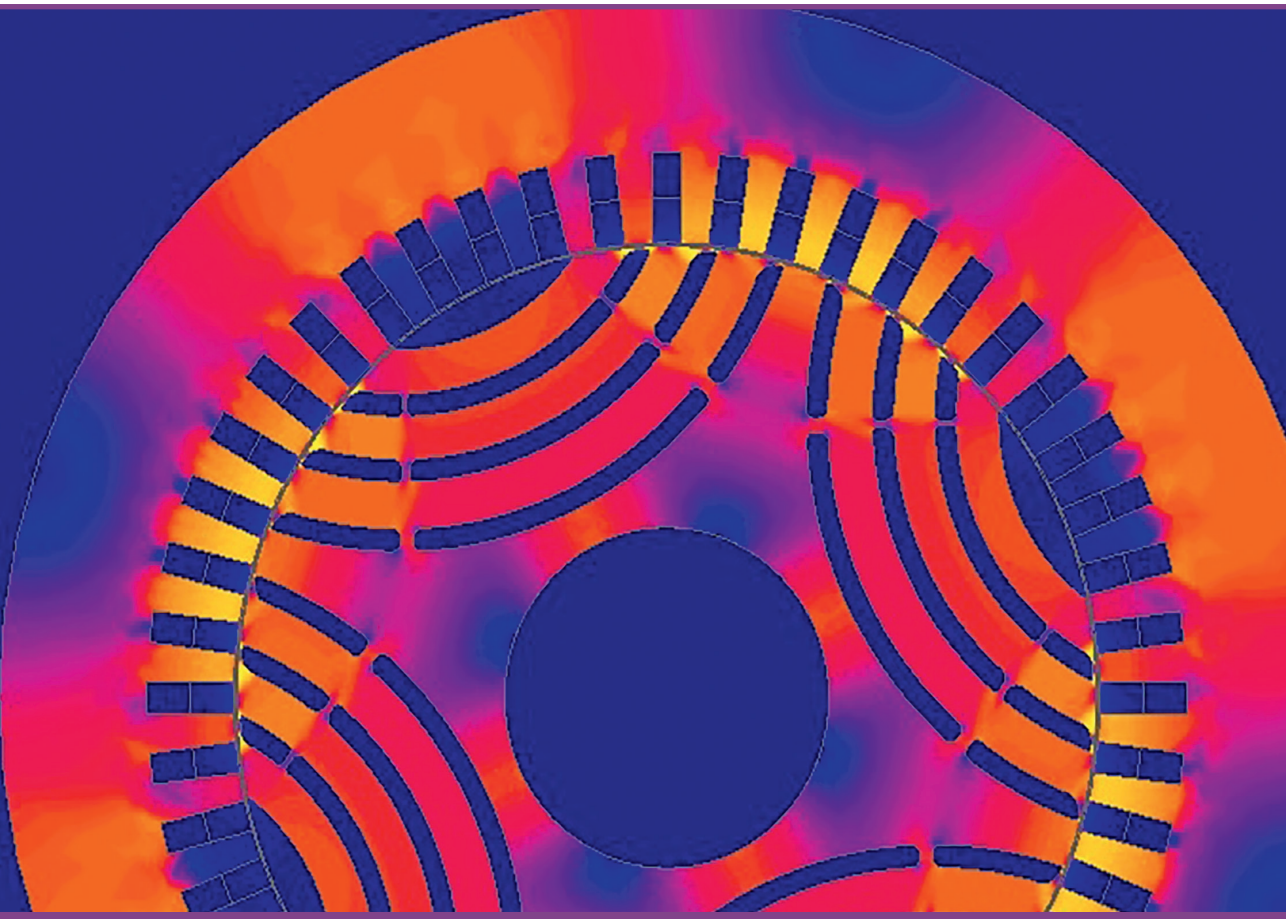

RTU Press
Riga 2025

RIGA TECHNICAL UNIVERSITY
Faculty of Computer Science, Information Technology and Energy
Institute of Industrial Electronics, Electrical Engineering and Energy

Kārlis Gulbis
Doctoral Student of the Study Programme "Smart Power Systems"

DEVELOPMENT OF THE SYNCHRONOUS RELUCTANCE MOTOR FOR APPLICATION IN PUBLIC TRANSPORT

Summary of the Doctoral Thesis

Scientific supervisor
Professor Dr. sc. ing.
ANDREJS PODGORNOVS

RTU Press
Riga 2025

Gulbis K. Development of the Synchronous Reluctance Motor for Application in Public Transport. Summary of the Doctoral Thesis. – Riga: RTU Press, 2025. – 54 p.

Printed accordingly to the decision of Promotion Council "P-14" of February 19, 2025, Minutes No. 04030-9.12.2/2.

Cover picture by Kārlis Gulbis.

https://doi.org/10.7250/9789934371875
ISBN 978-9934-37-187-5 (pdf)

DOCTORAL THESIS PROPOSED TO RIGA TECHNICAL UNIVERSITY FOR PROMOTION TO THE SCIENTIFIC DEGREE OF DOCTOR OF SCIENCE

To be granted the scientific degree of Doctor of Engineering Sciences, the present Doctoral Thesis has been submitted for defence at the open meeting of RTU Promotion Council on June 18, 2025 at the Faculty of Computer Science, Information Technology and Energy of Riga Technical University, Azenes street 12/1, room 508.

OFFICIAL REVIEWERS

Professor Dr. habil. sc. ing. Leonīds Ribickis,
Riga Technical University

Senior researcher Dr. sc. ing. Svetlana Orlova,
Institute of Physical Energetics, Latvia

Research Professor Ph. D. Toomas Vaimann,
Tallinn University of Technology, Estonia

DECLARATION OF ACADEMIC INTEGRITY

I hereby declare that the Doctoral Thesis submitted for review to Riga Technical University for promotion to the scientific degree of Doctor of Science (Ph. D.) is my own. I confirm that this Doctoral Thesis has not been submitted to any other university for the promotion to a scientific degree.

Kārlis Gulbis ……. (signature)
Date: ……

The Doctoral Thesis has been written in Latvian/English. It consists of an Introduction; 3 chapters; Conclusions; 61 figures; nine tables; and one appendix; the total number of pages is 104. The Bibliography contains 61 titles.

Contents

1. GENERAL DESCRIPTION OF THE THESIS

Relevance of the Topic

The increasing demands on the efficiency of electrical machines and the availability of semiconductor electronic control systems led to a situation in which long-established solutions were in many cases no longer the best solutions, such as the squirrel-cage induction motor on factory benches, the wound rotor induction motor in crane machinery or the DC motor in traction transport. The availability of semiconductor electronic control systems makes it possible to use AC electric machines in variable speed applications such as transport drives. The modern demands on the efficiency of electrical machines are very difficult to meet using an induction motor. AC machines that meet modern efficiency requirements for electrical machines are permanent magnet machines and synchronous reluctance machines (SynRM). The main advantages of permanent magnet machine compared to the SynRM will be higher efficiency and higher specific power, but the main disadvantages will be comparatively higher material and production costs, sensitivity of the magnets to high temperatures and the risk of magnet demagnetisation, as well as the availability of permanent magnets which must be considered in a geopolitical context, given that China meets 98 % of the total European Union demand for rare earth material.

The development and design of electrical machines is very much based on empirical coefficients that have been refined over the years, but the very different nature of the SynRM rotor from induction machines and synchronous machines with field winding means that previously known solutions for machine design are only partially applicable to the SynRM, applicable to the stator, and rotor geometry solutions have to be found anew. Importantly, the relevance of SynRM coincided with the availability and performance development of finite element mathematical modelling (FEM). The FEM method is widely used in SynRM research, development and design.

The European Green Deal and the move towards climate neutrality were presented in 2019 as a necessity and as an opportunity for economic growth, with 25 % of the European Union's long-term budget [1]. Currently, greenhouse gas emissions from the transport sector account for about 25 % of the European Union's total emissions, and for Europe to become the first climate-neutral region in the world by 2050, major changes are needed in the transport sector, where climate-neutral public transport will have a significant impact. The European Green Deal is more stringent for public land transport than for private transport, with all new urban transport, including new urban buses, required to be zero-emission vehicles by 2030, which is only possible through the electrification of urban public transport.

In this Thesis, SynRM has been chosen as the object of research because, in the author's opinion, SynRM is the best choice in Europe for the drive of grid-connected public transport. The SynRM rotor consists of only electrical steel, has no active materials, and is easy to manufacture, repair or replace. The SynRM rotor is suitable for the harsh operating conditions typical of transport drive systems. For mains-powered transport, efficiency and power density are less important compared to battery-powered transport. SynRM does not have permanent magnets, permanent magnet materials such as neodymium (Nd), praseodymium (Pr),

dysprosium (Dy) and terbium (Tb) whose extraction is associated with significant issues of environmental degradation in proportion to the small amount of rare earth material extracted from mines, ethical issues and security of supply chains. The European Union has taken significant steps to address the rare earth material problem, but even in optimistic scenarios the European Union would only be able to supply 20 % of its own rare earth needs in 2030 [2], which, in the author's view, is a significant argument for the use of permanent magnet alternatives especially in the drive of grid-connected public transport.

SynRM has significant advantages, as listed above. However, disadvantages include lower specific power compared to other machine types, which can be addressed by improving the cooling system efficiency, using an open machine design or using a high-performance cooling system for a closed machine design. The Thesis proposes to increase the specific power of the SynRM by using an innovative cooling method, *the heat loops thermosyphon* (*HL*), based on the change of the coolant state of a matter in the evaporator from liquid to gas and in the vapour condenser from gas to liquid. SynRM is particularly suitable for forced cooling methods because the main losses of the machine, or the heat to be dissipated, are directly in the stator, which increases the efficiency of the cooling method.

The heat loops thermosyphon is a closed-loop, passive, low-loss, heat transfer system, with no additional energy consumption for heat circulation, which makes it possible to produce an electrical machine of closed design and without the need for additional protection of the electric motor from the environment. During the winter heating season, the heat from the SynRM can be used to heat transport cabins, reducing the overall electricity consumption of the vehicle.

Aim of the Thesis

The Thesis aims to develop a high-performance closed-design synchronous reluctance machine achieved by the application of an innovative cooling method, the heat loops.

A significant part of the Thesis is devoted to the design of SynRMs with the aim that the Thesis becomes a source in Latvian for the reader, student or electrical design engineer, to design high-performance SynRMs.

Tasks

- To develop a description of the design of synchronous reluctance machines.
- To develop a method for the calculation of SynRM parameters, which can be used to accurately calculate the parameters of the SynRM to be designed already at the design stage.
- Design, manufacture and test a 180 kW SynRM prototype.
- Test the performance of the 180 kW SynRM using an innovative cooling method – heat loops.

Object and scope of the study

The object of the study is a synchronous reluctance machine designed to drive public transport. The Thesis is limited to the SynRM itself without considering the frequency converter feeding it, assuming that the frequency converters and their algorithms required for the SynRM operation are well studied and commercially available, which have been studied in other studies

[3]. The Thesis considers a SynRM whose stator is similar to that of a typical three-phase AC machine, and the SynRM rotor has no active elements.

In the framework of the study, a 180 kW SynRM was designed, fabricated and experimentally tested to replace an asynchronous motor in a public transport drive.

A 180 kW SynRM model with an innovative cooling method – heat loops – was produced and experimentally tested in the framework of the study.

Novelty of the research

A method for calculating the parameters of the SynRM machine has been developed, which takes into account the interaction between direct and quadrature axis magnetising forces. The developed method allows for more accurate calculation of the motor parameters at the design stage compared to standard calculation methods. The developed method improves the design result, based on which the designer can assess with higher certainty whether the design result satisfies the design task or whether additional optimisation steps are necessary.

A closed-loop SynRM has been developed using an innovative cooling method, heat loops, replacing SynRM with IC01 cooling.

Practical relevance

Within the framework of the research, the largest electrical machine building company in Latvia, JSC "Riga Electrical Engineering Plant", produced a 180 kW SynRM machine, which gave the company practical experience in the manufacture of this type of machine. Prior to the project, the company specialised mainly in induction and DC traction motors.

As part of the research, "Allatherm" Ltd had the opportunity to apply its technological skills in the development of cooling systems to the cooling of a high-power traction electric machine. The company's technologies have been mainly applied in electronics cooling.

The SynRM design description developed in the framework of the research can be used as a guideline for developing this type of electrical machine.

Hypotheses put forward in the Thesis

The calculation of SynRM parameters at the design stage can be approximated to the actual one, taking into account the magnetic cross-saturation according to the calculation algorithm presented in the study. The hypothesis is tested in Chapters 2 and 4, where the calculation method is presented in Chapter 2 and the results of the calculation method are compared with the experimental results in Chapter 4.

The technical performance of the SynRM can be improved by using an innovative cooling method, the heat loops. The hypothesis is tested in Chapters 3 and 4, where Chapter 3 describes the application of the method and Chapter 4 describes the experimental results.

Research tools and methods

The Thesis uses a numerical research method. The mathematical modelling of the magnetic fields in the study is performed using the finite element modelling software *Altair Flux*. Finite element mathematical modelling is a widely used tool for the modelling and calculation of magnetic fields. The results of the finite element mathematical modelling have been processed using the basic equations of electromagnetic processes and well-known computational methods.

The Thesis uses a laboratory study method. Laboratory experiments with physical models have been carried out in the framework of the study in order to validate the results of the numerical method.

Approval

In the framework of the Thesis, seven scientific publications have been published in the last eight years. The author has actively contributed to two ERDF projects that pertain to the subject of the Thesis. The research endeavours have encompassed the development and experimentation of a 180 kW SynRM, two SynRM models (1/12 segments) equipped with a heat loops cooling system, and a full 180 kW SynRM that is also fitted with a heat loops cooling system.

Publications

1. Gulbis, K., Podgornovs, A., Bižāns, A., Lavrinoviča, L. **Increasing the Power Density of 180 kW Synchronous Reluctance Motor by Implementing Loop Heat Pipe Cooling.** In: 2023 3rd International Conference on Electrical, Computer, Communications and Mechatronics Engineering (ICECCME 2023), Spain, Santa Cruz de Tenerife, 19–21 Jul. 2023.
2. Lavrinoviča, L., Gulbis, K., Podgornovs, A., Bižāns, A. **Analysis of the Heat Dissipation of Synchronous Motor with Reluctance Rotor with Goal of Power Density Increasing.** In: 2023 International Conference on Electrical Drives and Power Electronics (EDPE 2023): Proceedings, Slovakia, The High Tatras, 25–27 Sept. 2023.
3. Gulbis, K., Brakanskis, U., Kamoliņš, E., Gorobecs, M., Potapovs, A., Sējējs, K., Zarembo, J., Burenin, V. **Analysis of Test Results of the Developed Synchronous Reluctance Motor for Public Transport Application.** Latvian Journal of Physics and Technical Sciences, 2022, Vol. 59, No. 4, pp. 25–41.
4. Lavrinoviča, L., Podgornovs, A., Bižāns, A., Gulbis, K. **Overview of Thermal Loads Distribution in Traction Electric Machines and Conditions for Forced Cooling of Their Parts.** In: 2022 International Conference on Electrical, Computer and Energy Technologies (ICECET 2022), Czechia, Prague, 20–22 Jul. 2022.
5. Kamoliņš, E., Gorobecs, M., Burenin, V., Gulbis, K., Potapovs, A., Brakanskis, U., Zarembo, J., Sējējs, K. **180 kW Synchronous Reluctance Motor for Mass Transit Electrical Traction Application.** In: 2021 23rd European Conference on Power Electronics and Applications (EPE'21 ECCE Europe), Belgium, Ghent, 6–10 Sept. 2021.
6. Gulbis, K., Brakanskis, U., Kamoliņš, E., Zarembo, J. **Parameter Calculation Method of Synchronous Reluctance Motor Including Cross Magnetic Saturation.** In: 2020 IEEE 61st Annual International Scientific Conference on Power and Electrical Engineering of Riga Technical University, RTUCON 2020.
7. Gulbis, K., Kamoliņš, E., Brakanskis, U**. Synchronous Reluctance Machine with Improved Design of Rotor Mechanical Strength Connections**. In: 2016 IEEE 4th Workshop on Advances in Information, Electronic and Electrical Engineering (AIEEE 2016): Proceedings, Lithuania, Vilnius, 10–12 Nov. 2016.

Projects

1. ERDF co-financed project No. 1.1.1.1/20/A/116 "Smart Thermal Management in Electric Drives with Built-In Heat Pipes/Loops for Better Reliability and Functionality".
2. ERDF co-financed project No. 1.1.1.1.1/18/A/055 "Development of a New Generation Synchronous Reluctance Electric Motor ".

2. SYNCHRONOUS RELUCTANCE MACHINES AND THEIR DESIGN

2.1. History and development of SynRM

The electric motor with salient rotor poles, no rotor winding and no permanent magnets, which develops torque based on the magnetic asymmetry (saliency) of the rotor, is one of the oldest electric machines. In the 20th century, reluctance machines were used in niche applications such as positioning machines in the textile industry and other applications where it was particularly important to maintain a precise pitch or speed, but the developed torque, efficiency and power factor were of secondary importance. The late 20th century saw the development of reluctance stepper motors, with which the name reluctance machine is associated until the second decade of the 21st century, when the first mass-market-ready synchronous reluctance machines became commercially available [4]. The synchronous reluctance machine with air barriers to prevent q-axis flux is a 100-year-old solution presented by Kostko in 1923 [5]. In the late 20th century, the fundamental issues of SynRM were extensively studied. A low-pulsation SynRM rotor model is patented [6], which is the basis for the first mass-produced SynRMs that reached consumers in 2011.

In the history of SynRM development, it has long been assumed that the ability to start and run the motor connected directly to the grid is a prerequisite for widespread motor adoption, for which asynchronous starting is the most commonly proposed solution. Given the availability of control systems and the increased demand for control systems from consumers, it can be predicted that grid start will be a requirement for niche applications in the future rather than an existential requirement for SynRM applications.

2.2. Typology of SynRM

The current most popular rotor types for SynRM are summarised in Fig. 2.1.

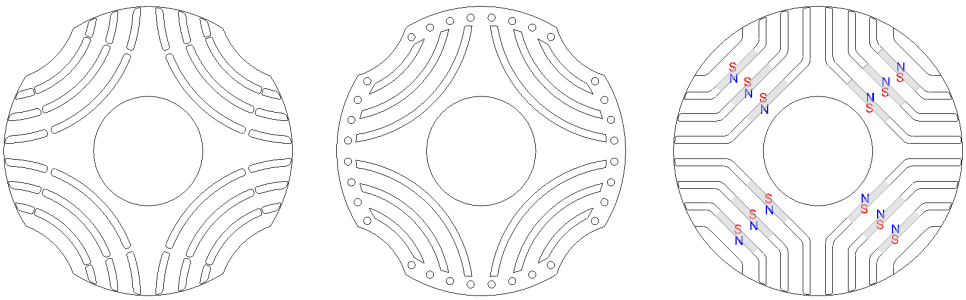

a) SynRM b) DOLSynRM c) PMASynRM

Fig. 2.1. Synchronous reluctance motor rotor designs:
a) rotor with non-magnetic (air) barriers (SynRM) operates with a frequency converter;
b) grid-connected motor, rotor design with air barriers and short-circuited squirrel cage starting windings (DOLSynRM);
c) rotor design with magnets in air barriers (PMASynRM).

2.3. SynRM operating principle and electromagnetic torque

The electromagnetic torque of the SynRM can be expressed by Equation (2.1), where it depends on the applied voltage and its frequency, the inductive reactance of the direct axis X_d and quadrature axis X_q and the load angle Θ. The larger the ratio between the inductive resistances $K_{d/q} = X_d/X_q$ (saliency ratio), the larger the electromagnetic torque. The maximum electromagnetic torque will be reached at a load angle of 45°.

$$T = \frac{3V^2}{2\omega} \times \left(\frac{X_d - X_q}{X_d X_q}\right) \times \sin 2\Theta \qquad (2.1)$$

The direct and quadrature axis reactances contain the winding leakage reactance X_s, which are assumed to be the same for both components. The direct and quadrature inductive reactances are to be calculated from the winding electromotive force (emf) and current. The emf can be calculated from the magnetic flux analytically or by FEM.

The shape of the SynRM electromagnetic torque curve depends on machine geometry parameters such as air gap width, air gap uniformity, pole pitch, stator slot and rotor air barrier dimensions and their relationship to each other. In addition to the geometrical parameters, the winding pitch and the electrical parameters will influence the shape of the electromagnetic torque curve. As a result, the electromagnetic torque versus load angle curve shown in Fig. 2.2 will be different from that calculated by Equation (2.1) if the torque is calculated assuming constant direct and quadrature field resistances. The maximum torque of the model in Fig. 2.2 corresponds to a critical load angle of 53°. The critical load angle depends on the design of the magnetic system of the machine, in particular, the pole pitch.

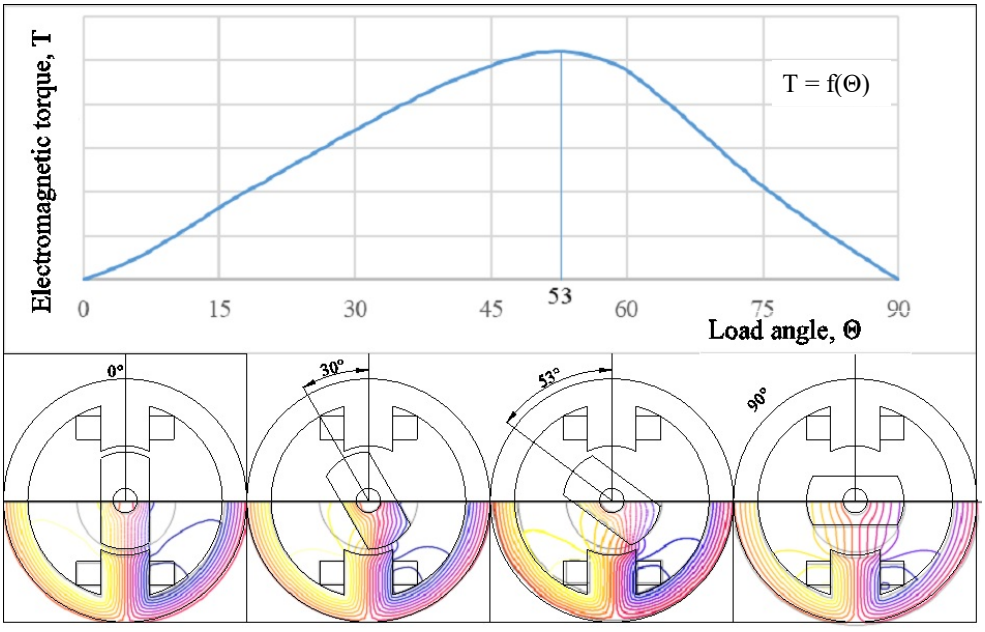

Fig. 2.2. Electromagnetic torque versus load angle.

2.4. SynRM parameters

2.4.1. Causes, effects and ways of limiting electromagnetic torque ripple

Torque ripple in an electrical machine can be attributed to a mechanical or electromagnetic cause. Such causes may include mechanical load, rotor centring misalignment, control equipment, and magnetic circuit asymmetries. Regardless of the underlying cause, the ripple invariably leads to mechanical vibration, noise, and stability problems in the synchronous machine.

The phenomenon of mechanical vibrations has been observed to induce detrimental effects on various components of machinery, including bearings, the drive mechanism, and fastening mechanisms. Acoustic pollution, a by-product of mechanical vibrations, is a subject that has garnered significant attention. The utilisation of switched reluctance motors, for instance, has been constrained by the noise emanating from torque oscillations. The economic rationale for mitigating noise emissions is compelling, as machines that operate with minimal noise do not necessitate the implementation of additional sound attenuation measures. Machine instability may arise from the control equipment's inability to align the expected torque value with the actual value, resulting in a displacement due to torque ripple. The present study focuses on electromagnetic torque ripple generated by a magnetic system, with the mechanical cause of the ripple being analogous to that of a synchronous reluctance motor and other electric motors. Oscillations due to magnetic asymmetry are primarily caused by the interaction between the stator slots and the rotor barriers. The design of the magnetic system can mitigate the torque ripple caused by the interaction between the stator slots and the rotor air barriers. SynRM rotor designs can exhibit significant electromagnetic torque ripple, which cannot be eliminated by stator or rotor offset and stator winding pitch shortening alone. The key to designing a SynRM with low electromagnetic torque ripple is the development of the correct rotor geometry, which includes the ratio of the number of stator slots to the number of rotor air barriers, the rotor mechanical strength bridges and the shape of the rotor air barriers. The reduction of the electromagnetic torque ripple by considering the ratio of the number of stator slots to the number of rotor air barriers has been addressed in the literature [6], [7].

2.4.2. Factors affecting the efficiency ratio

The SynRM benefits from the absence of electrical losses in the rotor, a significant advantage over an induction machine [8]. However, magnetic losses are comparable to those of other electrical machines. The SynRM exhibits a higher current due to its low power factor, resulting in increased electrical losses compared to a permanent magnet machine.

A key benefit of the SynRM over an induction motor is its higher efficiency. It is difficult to design an induction motor to comply with efficiency class IE4, the energy efficiency class being assigned according to EN 60034-30-1:2014 "Rotating electrical machines – Part 30-1: Efficiency classes of line operated AC motors (IE code)". This can be achieved by increasing the size of the induction motor and the amount of copper and steel. Looking at the performance of ABB, one of the largest manufacturers of electrical machines: from 2011, SynRMs were

offered with IE4 class compliance without increasing the frame size; in 2019, SynRMs were offered with potential IE5 class compliance; in 2024, ABB presented a press release on SynRMs with potential IE6 class compliance, the so-called "*hyper-efficiency*" class, e.g. IE6 22 kW $2p = 4$ motor efficiency is 95.8 % [9].

A modern SynRM is designed to operate with a frequency converter, so it is useful to consider both the efficiency of the motor and the overall efficiency of the drive system, which is isolated in a separate standard IEC 60034-30-2:2016 "Rotating electrical machines – Part 30–2: Efficiency classes of variable speed AC motors (IE-code)".

2.4.3. Factors affecting the power factor

Historically, SynRM has been characterised by a significant drawback in the form of a low power factor. In the context of a contemporary SynRM driven by a frequency converter, this low power factor gives rise to two key consequences. Firstly, the selection of a larger frequency converter becomes imperative to match current rather than active power. Secondly, efficiency is reduced due to electrical losses or winding cross-section is increased, which in turn necessitates larger motor dimensions.

The power factor of a SynRM is determined by the air gap width and magnetic asymmetry (saliency ratio). It has been demonstrated that designs exhibiting higher magnetic asymmetry are associated with higher power factors [10], [11].

2.5. SynRM design

The SynRM stator consists of slots in which a three-phase winding is inserted, teeth through which the magnetic flux is directed towards the rotor and a yoke, and the dimensions of these stator elements and winding are similar to those of permanent magnet synchronous and induction motors. SynRM stator design can be achieved with well-developed methodologies and manufactured with existing technologies for synchronous and induction machines. AC machine design methodologies have their nuances in each region, but are uniformly based on coefficients and ratios that have been empirically refined over decades. In contrast, SynRM rotor design is a relatively new necessity, emerging at the same time as finite element modelling (FEM) techniques became available and easy to use, which can very successfully replace the empirical coefficients previously very popular in design.

2.5.1. AC machine design

The design of electrical machines is an iterative procedure, the outcome of which depends on the objective functions of the electric motor and on the validating constraints related to temperature rise, starting current, starting torque, maximum torque, etc. The objective function may be the weight, cost of the active materials, the overall cost, efficiency or a weighted combination of all these factors. The design of AC machines, in particular induction motors, is explained extensively in references [11] and [12], which have been used extensively to define the reference points within the framework of this research.

2.5.2. SynRM design algorithm

The SynRM design algorithm is proposed in Fig. 2.3. The full description of the developed design flow chart is available in the Thesis. The contributions of [11]–[14] have been important in the development of the algorithm. The implementation of FEM in the design process is recommended, e.g. in the development of the optimal geometrical parameters of the SynRM, especially in the design of the SynRM rotor: selection of the width, number, shape and position of the rotor air barriers.

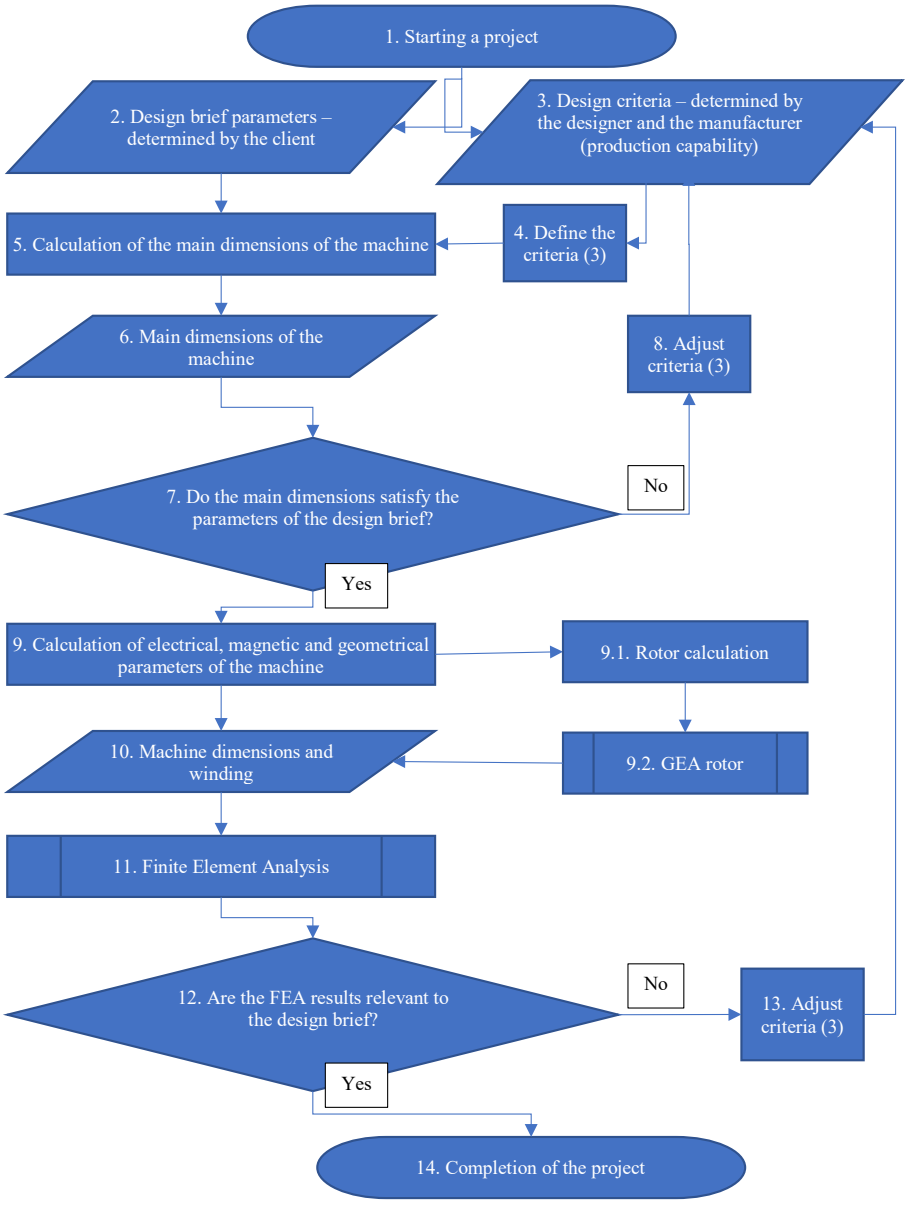

Fig. 2.3. SynRM design flow chart.

2.5.3. Main dimensions of SynRM

The sequence for calculating the main dimensions of the machine will be the same as for other AC machines. The sequence of calculations is based on an assumed machine utilisation – Esson factor C_0 [kW/m^3] [12]. The calculation algorithm will be similar, choosing instead of the Esson coefficient the linear load A and the magnetic induction in the air gap B_δ from the recommendations [11]. The differences between SynRM and AD or PMSM should be evaluated by choosing C_0, A, and B_δ.

2.5.4. SynRM windings and stator slots

SynRM winding calculation

The SynRM winding parameters can be calculated using the same methods as for other AC machines. Typical winding calculation methods are based on a number of empirical coefficients that may be inaccessible to the designer of a new type of machine, such as the SynRM, so it is proposed to include FEM-based optimisation steps in the SynRM winding calculation.

Single- or double-layer winding

SynRM can use single- or double-layer windings like other AC machines. Simplifying the choice, a single-layer winding has a higher peak electromagnetic torque and a simpler design, while a double-layer winding has a smaller torque ripple. For a four-pole machine, the recommended winding pitch reduction ratios are 5/6, 7/9, 10/12 or 12/15. Smaller pitch shortening does not sufficiently reduce torque ripple due to the increased complexity of the stator winding design and increased manufacturing costs. The proposed step-shortening ratios provide a reduction of the fifth and seventh MDS harmonics [15], [16].

SynRM's slot size calculation

As with other AC machines, the SynRM's slot dimensions will be mainly determined by the calculated winding dimensions and the manufacturer's technological capabilities.

2.6. Modern SynRM rotor design

The rotor of a modern SynRM is made of radially laminated sheets of electromagnetic steel with air barriers to restrict the q-axis magnetic flux (Fig. 2.4 b)). The air barriers in the SynRM rotor are designed to obtain a high magnetic resistance in the quadrature axis direction. The SynRM rotor with air barriers is characterised by a wide pole overlap of ~ 2/3 τ and a high saliency ratio $K_{d/q} > 4$, compared to the rotor of a salient pole synchronous machine without air barriers $K_{d/q} \sim 2$ (Fig. 2.4 a)). The manufacturing of a SynRM rotor with air barriers will be simpler compared to an axially laminated rotor (Fig. 2.4 c)). The design of the rotor will be mainly determined by the magnetic circuit. The mechanical strength requirements will have a minor influence on the design. Heating and cooling will not affect the rotor design.

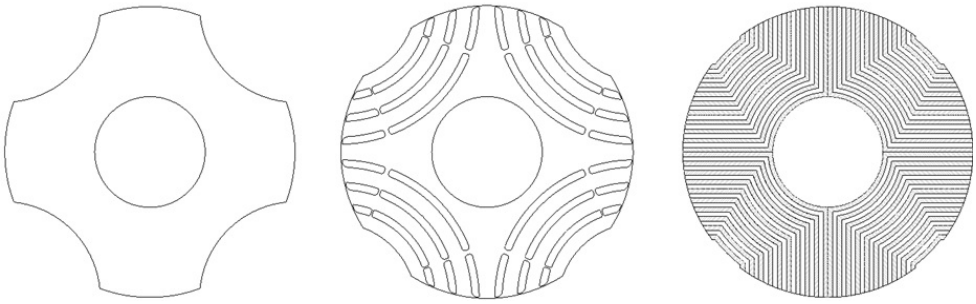

a) b) c)

Fig. 2.4. SynRM rotor designs: a) salient pole; b) non-magnetic air barrier; c) axially laminated electrical steel sheets.

The overwhelming majority of SynRMs in production have four poles. A rotor design with air barriers, characterised by a high saliency ratio and low electromagnetic torque ripple, is practically impossible for a two-pole machine. For six- (Fig. 2.5 a), b)) and eight-pole (Fig. 2.5 c)) machines, it is possible to design a rotor with air barriers, but the design will be characterised by a lower specific electromagnetic torque [17]. For six- and eight-pole machines, it is more complicated to design a rotor with a large number of barriers, because the barriers are narrow and of variable width.

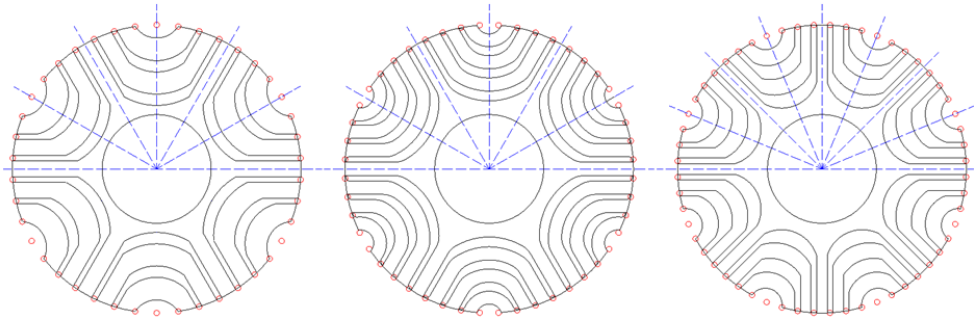

a) b) c)

Fig. 2.5. SynRM design with different numbers of poles and rotor air barriers: a) $2p = 6$, $N_r = 42$; b) $2p = 6$, $N_r = 48$; c) $2p = 8$, $N_r = 56$.

The calculation of the main dimensions, winding and stator of a SynRM does not differ significantly from an induction motor, the differences are in the values of the empirical coefficients adopted. The SynRM has no active elements in the rotor, so its calculation will be completely different from an induction or permanent magnet synchronous machine (Fig. 2.6).

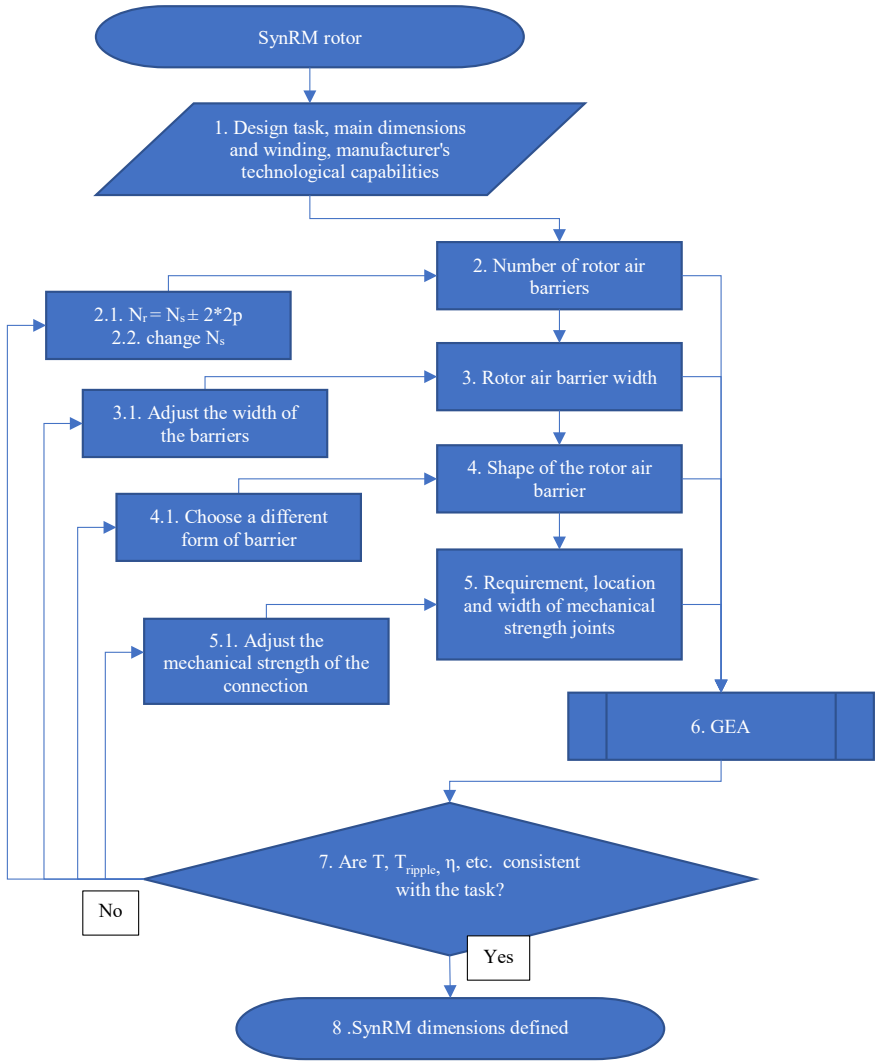

Fig. 2.6. SynRM rotor sizing algorithm.

2.6.1. Number of non-magnetic air barriers in the rotor

The number of non-magnetic rotor air barriers will depend on the number of poles, the number of stator slots, the size of the machine and the manufacturer's ability to create small rotor air barriers. A higher number of rotor air barriers will be characterised by higher magnetic asymmetry and lower electromagnetic torque ripple; as a limiting design with a very high number of flux-conducting channels and non-magnetic barriers, an axially laminated rotor can be considered (Fig. 2.4 c)).

Laminating the steel sheets axially instead of radially creates a layer of magnetic insulation between them, which is used to restrict the flux in the quadrature direction. The magnetic

asymmetry value $K_{d/q} \sim 10$ [18], [19] for axially laminated rotor structures is significantly higher compared to radially laminated air barrier rotor structures. However, the axially laminated rotor design has significant drawbacks. An axially laminated rotor is difficult to fabricate; each sheet will be a unique size. In Fig. 2.4 c), it can be observed that each successive sheet closer to the air gap is shorter than the previous one. The bending of the sheets must be ensured, which is particularly difficult in the part near the shaft. The sheets shall be secured to each other utilising axial bolts or other elements. It has been established that an axially laminated rotor is characterised by increased eddy currents. This phenomenon consequently results in elevated magnetic losses, which are estimated to be 2–3 times higher in comparison to those of a radially laminated rotor equipped with air barriers [19].

The manufacturing of a radially laminated rotor with a large number of air barriers is likely to be challenging due to the complexity of the flux-guiding channels, which are only a few millimetres wide. The mechanical robustness and high manufacturing precision of these channels are also questionable. The optimum number of rotor air barriers for high electromagnetic torque and low electromagnetic torque ripple can be determined from the number of stator slots, N_S, and the number of poles, following Equation (2.2) [6]. By following the equation, the higher harmonics of the magnetic flux density in the air gap caused by the interaction between the stator slot and the rotor air barrier and the resulting electromagnetic torque ripple are significantly reduced. The choice between a number of rotor air barriers greater or less than the number of stator slots (2.2) must be considered for each machine to be designed individually. Figure 2.7 c) shows that if $N_r = N_S$ is chosen, all rotor air barriers are placed directly against the stator slots, resulting in a large torque ripple, and such a design is not viable.

$$N_r = N_S \pm 2 \times 2p \text{ or } \frac{N_r}{p} = \frac{N_S}{p} \pm 4 \tag{2.2}$$

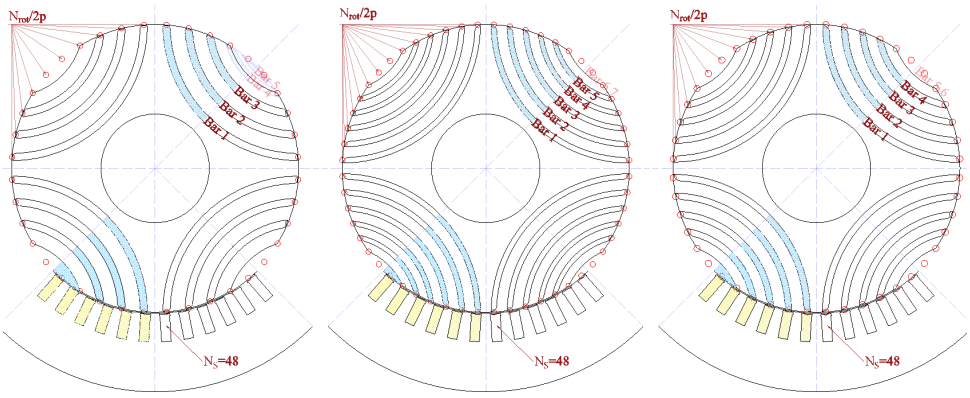

a) b) c)

Fig. 2.7. Number of air barriers, SynRM with $2p = 4$, $N_s = 48$:
a) $N_r < N_S$, $N_r = N_S - 2 \times 2p = 40$; b) $N_r > N_S$, $N_r = N_S + 2 \times 2p = 56$; c) $N_r = N_S$, $N_r = N_S = 48$.

2.6.2. Width of rotor non-magnetic air barriers and flux channels

The ratio of the width of the rotor's non-magnetic air barriers to the width of the flux-conducting channels (2.3) will affect the magnetic asymmetry of the machine and the electromagnetic torque developed by the machine. Magnetic asymmetry determines not only the electromagnetic torque but also the power factor, current and losses. In the first iteration of the rotor calculation, the ratio of the width of the non-magnetic air barriers and the width of the flux-conducting channels can be assumed based on the recommendation $K_{gb/Fe} \in (0.3–0.5)$ [10]; similar values are recommended in [18]. For the selection of the rotor barrier and the width of the flux-guiding channels, it is recommended to solve the optimisation problem with several parameters to be optimised, such as maximising the peak torque and the power factor.

The SynRM rotor non-magnetic air barrier and flux-guiding dimensions are denoted in Fig. 2.8, where the dimensions b_{gb} – air barrier width and b_{Fe} – flux-guiding channel width are distributed along the q-axis and at the air gap δ, additionally denoted $b_{iz\,q}$ – cut-out along the q-axis at the air gap and $\tau_{(\pi)}$ – rotor tooth section.

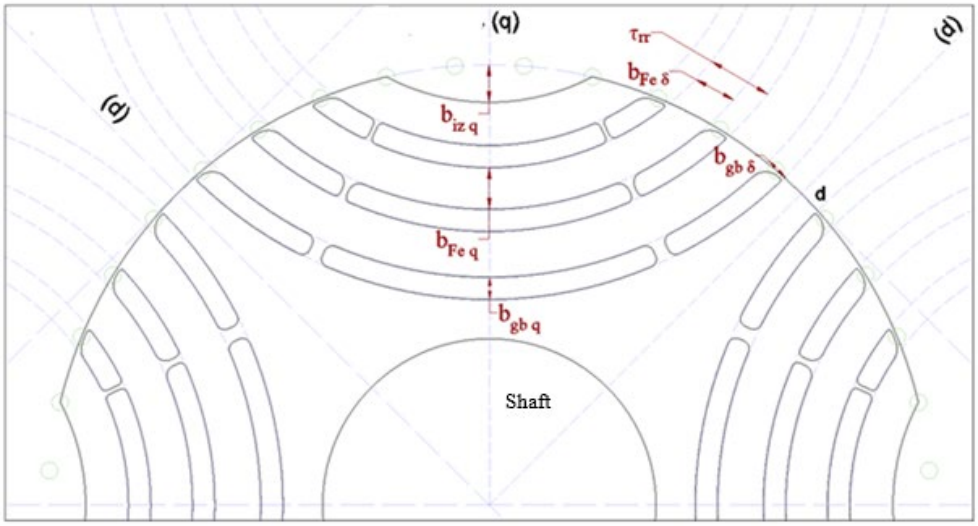

Fig. 2.8. Dimensions of rotor air barriers and flux channels.

It is preferred that rotor flux conducting channels have a constant width throughout the length of the channel $b_{Fe\,q} = b_{Fe\,\delta}$. Almost all $b_{Fe\,\delta}$ are of the same width, so that the channel closest to the cut-out can be designed with a slightly increased $b_{Fe\,\delta}$ to provide the desired pole pitch. Almost all $b_{Fe\,q}$ are of the same width, with a slightly reduced width on the q-axis the closest $b_{Fe\,q}$ to the shaft can be formed, the width is determined by FEM, the criterion being equal magnetic flux density distribution in all $b_{Fe\,q}$. A constant width of b_{Fe} throughout the channel ensures a uniform distribution of the magnetic flux density in the channel without generating additional higher harmonics.

The shape of the rotor non-magnetic air barriers may be of uniform width, $b_{gb\,q} = b_{gb\,\delta}$, along the entire length or of increasing width in the q-axis direction, $b_{gb\,q} > b_{gb\,\delta}$. A structure with an

air barrier wider at the air gap than on the q-axis is considered undesirable, in which case it should be examined whether too small a pole pitch and too large a cut-out towards the q-axis – $b_{iz\,q}$ – have been chosen. SynRM with a pole number greater than 4 for virtually all designs $b_{gb\,q} > b_{gb\,\delta}$. The necessity for a cut-out along the q-axis at the air gap $b_{iz\,q}$ shall be determined by the designer through the following considerations:

- the requirement for the rotor to be shaped like a perfect cylinder, as dictated by the manufacturing technology;
- the sufficiency of the design's mechanical strengthening, in the absence of a cut-out;
- the capacity of the design to produce sufficient saliency, without the formation of a cut-out.

Without the cut-out (Fig. 2.9 b)), the air barriers and flux channels at the air gap along the q-axis can form complex geometries with small dimensions and very sharp angles, which will be difficult to manufacture, such as barriers 4 and 5 in Fig. 2.7 a).

When the SynRM is designed as recommended in [6], the width of the rotor air barrier and the flux-guiding channel section τ_{rr} is kept constant.

The ratio of the width of the flux-conducting channels and air barriers (2.3) is expressed as the ratio of the width of all non-magnetic air barriers and cut-outs to the total width of the barrier, cut-out and steel.

$$K_{gb/Fe} = \frac{\sum b_{gb} + b_{iz}}{\sum b_{gb} + b_{iz} + \sum b_{Fe}} \tag{2.3}$$

2.6.3. Shape of non-magnetic air barriers

The shape of the rotor air barriers is usually trapezoidal (Fig. 2.9 c)) or arch (Fig. 2.9 a)). The shape of the air barrier may be a separate optimisation task. The choice of air barrier shape will be influenced by the manufacturer's capabilities, which will depend on the equipment available to the manufacturer and the rotor manufacturing technology chosen. The required shaft diameter will have a significant influence on the shape of the barrier. Trapezoidal or arch barriers can be of fixed barrier width or $b_{gb\,q} > b_{gb\,\delta}$. Trapezoidal barriers are often designed with rounded edges (Fig. 2.9 b)) to limit the non-uniform distribution of magnetic flux density. For arc-shaped barriers, the determination of the centre of the arc will be essential.

When air barriers have an arch design and all barriers have a common centre, the torque ripple is reduced compared to trapezoidal air barriers, e.g. 180 kW, $p = 2$, $f = 50$ Hz SynRM at rated load has 4 % smaller electromagnetic torque ripple [20]. When designing PMASynRMs, it is recommended to choose trapezoidal barriers.

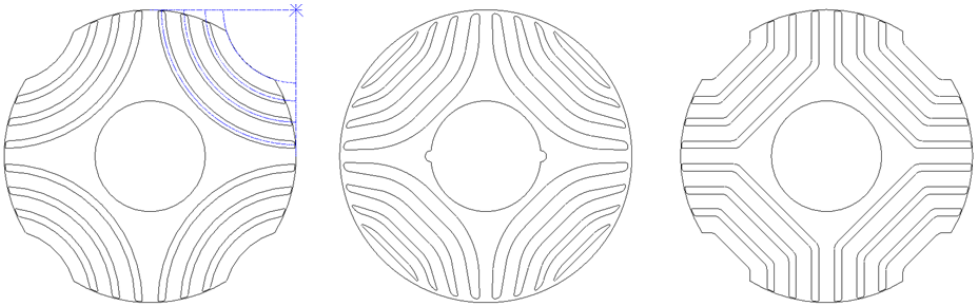

a) b) c)

Fig. 2.9. Shape of air barriers: a) arch with common centre; b) trapezoidal with rounded corners; c) trapezoidal.

2.6.4. Mechanical strength connections

Mechanical strength connections are designed to ensure the mechanical strength of the rotor. As the size of the machine increases, larger connections must be provided as the mechanical forces on the steel parts of the rotor increase. The mechanical strength connections reduce the saliency ratio and reduce the peak electromagnetic torque. While the mechanical strength connections at the air gap have a positive effect on the electromagnetic torque ripple, which is slightly reduced, e.g. in [21] and [22], it is estimated that the mechanical strength connections reduce the peak torque by 7 % and the torque ripple by 2 %. Similar observations, decomposing the effect of mechanical strength joints at the air gap and along the q-axis, are presented in [18]. A separate optimisation problem based on mechanical and electromagnetic calculations is recommended for mechanical strength connections.

Typical mechanical connection types for a modern SynRM design are: at the air gap in Fig. 2.10, denoted by width $b_{meh\,\delta}$ and air barrier separating in Fig. 2.10 b), denoted by width $b_{meh\,q}$ if the attachment is directly on the quadrature axis, or in Fig. 2.11 a), denoted by $b_{meh\,\alpha}$ if the attachment is offset from the quadrature axis by angle α_{meh}. The need, location, width and number of mechanical connections shall be determined by the rotor mechanical strength calculation. For example, the 1.5 kW, $p = 2$ SynRM (Fig. 2.9 b)), manufactured by KSB, one of the largest manufacturers of electrical machines and pumps, has only mechanical strength connections at the air gap $b_{meh\,\delta}$. Mechanical strength connections of different shapes have also been investigated, which make the rotor more complex to fabricate but are characterised by a higher saliency ratio, e.g. a specific shape (Fig. 2.11 c)) increases saliency ratio by 5 % compared to (Fig. 2.11 a)) design [21], or for example, the "dovetail" shape investigated in [23].

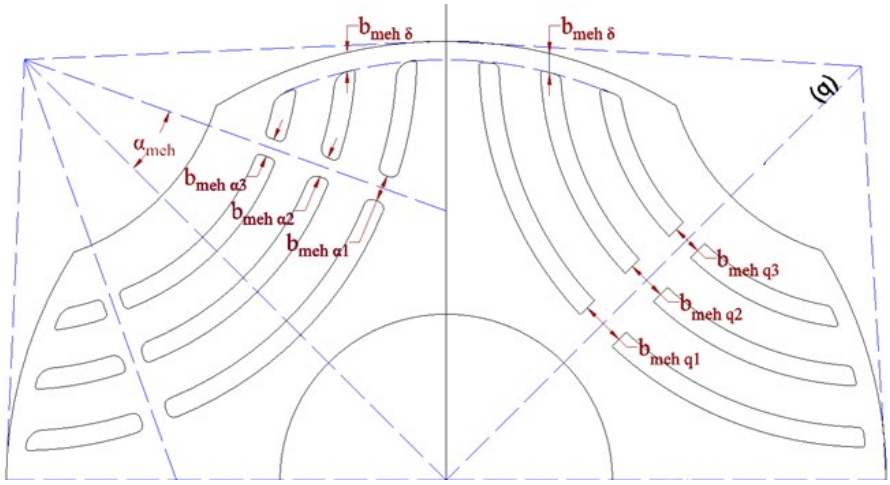

Fig. 2.10. Illustrative sketch of mechanical strength connections and their main dimensions: a) q-axis offset connection; b) q-axis connection.

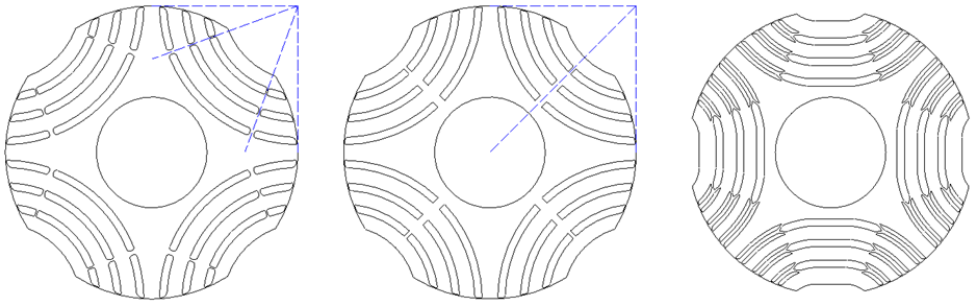

Fig. 2.11. Location and shape of mechanical strength connections: a) shifted from the q-axis; b) on the q-axis; c) connections with a complex shape.

2.6.5. Pole pitch

The rotor pole pitch will influence the maximum electromagnetic torque to be developed, the electromagnetic torque ripple and the load angle at which the maximum electromagnetic torque will be developed. Larger pole pitch machines will be characterised by smaller electromagnetic torque and reduced electromagnetic torque ripple [18]. According to [13], it is recommended to choose the pole pitch $\tau_p/\tau \sim 2/3$. In practice, several manufacturers choose rotors with $\tau_p/\tau = 1$, e.g. KSB 1.5 kW, $p = 2$ SynRM (Fig. 2.9 b)), thus the rotor is an ideal cylinder, which can be a necessity or optimisation of the manufacturing process.

2.6.6. Rotor skewing

Similar to an induction motor, the geometry of the stator and rotor slots creates higher harmonics in the air gap, which have a negative effect on the performance of the motor,

including causing electromagnetic torque ripple. In order to limit the higher harmonics caused by the slots, the stator or rotor of the SynRM can be designed with an axial offset. The rotor offset is mostly used. Stator offset is a technologically complex process involving the assembly of the steel stack, isolation of the slots and insertion of the winding, after which the stator stack is rotated, or offset, then fixed and impregnated together with the winding [11]. The SynRM rotor has no active elements, which is a major advantage for skewing the rotor. The rotor can be skewed by each electrical steel sheet (Fig. 2.12 a)), which has a greater effect on limiting the higher harmonics but is more complex and expensive to produce, or by dividing the rotor into segments (Fig. 2.12 b)).

The maximum effect of the offset on limiting the electromagnetic torque ripple is usually by about one stator slot. The offset will reduce the electromagnetic torque developed by the SynRM; the larger the offset, the smaller the developed torque. By skewing the rotor, air barriers form a fan-like design, and the air barriers will create forced air circulation with a minor cooling effect [24].

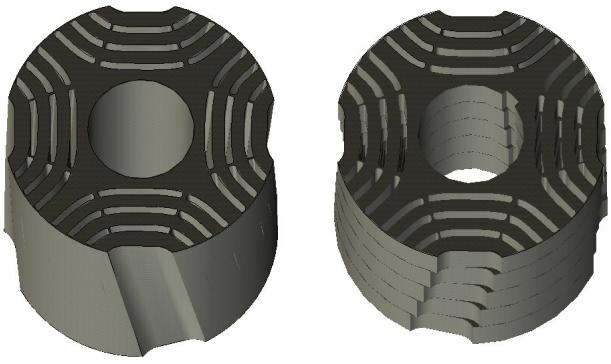

Fig. 2.12. SynRM with skewed rotor: a) skewing each sheet of electrical steel by a small angle; b) dividing the rotor into segments and skewing the segments.

2.7. SynRM parameter calculation

Calculation algorithm

An algorithm is proposed to calculate the reactances x_{ad}, x_{aq} and the load angle Θ, whereby the reactances are calculated from the FEM results taking into account the magnetic cross saturation and magnetic losses. The calculation algorithm does not require reactances to be expressed as a function of a given axis current. A new calculation algorithm, presented in [25], is proposed; the method is complemented by the consideration of magnetic losses. The magnetic losses can be calculated from: the magnetic flux density in the stator teeth B_z and yoke B_j obtained by FEM; the mass of the tooth and yoke of electrical steel; or in the FEM subroutine by calculating the Bertotti losses.

An algorithm is proposed based on which the resistances x_{ad}, x_{aq} and the load angle Θ are the design values. The resistances are calculated and need not be expressed as a function of the

currents. The angle Θ is calculated taking into account the effect of I_d on x_{aq} and the effect of I_q on x_{ad}.

The algorithm is based on sinusoidal alternating voltages. Machine design calculations are usually carried out assuming a sinusoidal AC voltage [13]. The developed algorithm differs from the Kamper method [26] in that the reactances are determined by calculating the electromagnetic torque with a FEM, and the reactances of the armature direct field x_{ad} and quadrature field x_{aq} are determined according to the vector diagram (Fig. 2.13).

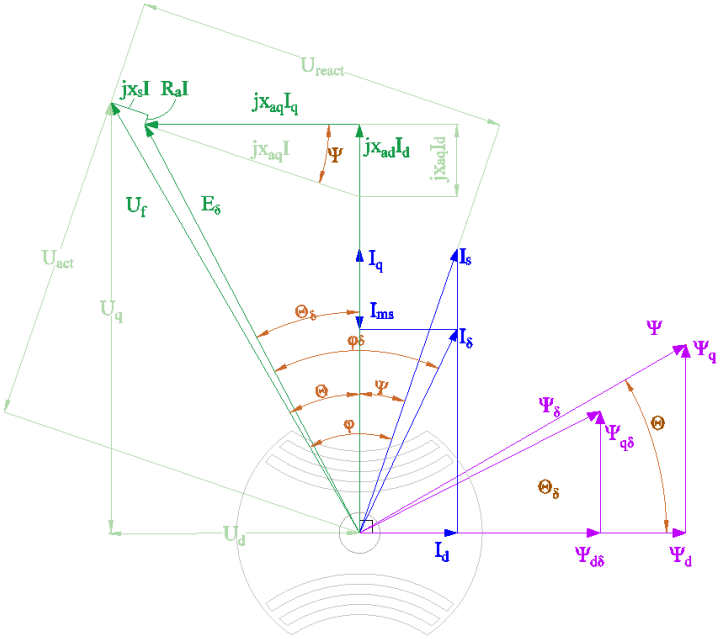

Fig. 2.13. 180 kW SynRM vector diagram, I_N = 372A, U_N = 420V, nominal load mode.

Algorithm calculation sequence

The vector diagram of a synchronous reluctance machine for the algorithm is shown in (Fig. 2.13). The sequence of operations of the algorithm is shown graphically in the flow chart (Fig. 2.14). The algorithm includes a numerical calculation part and a FEM calculation part.

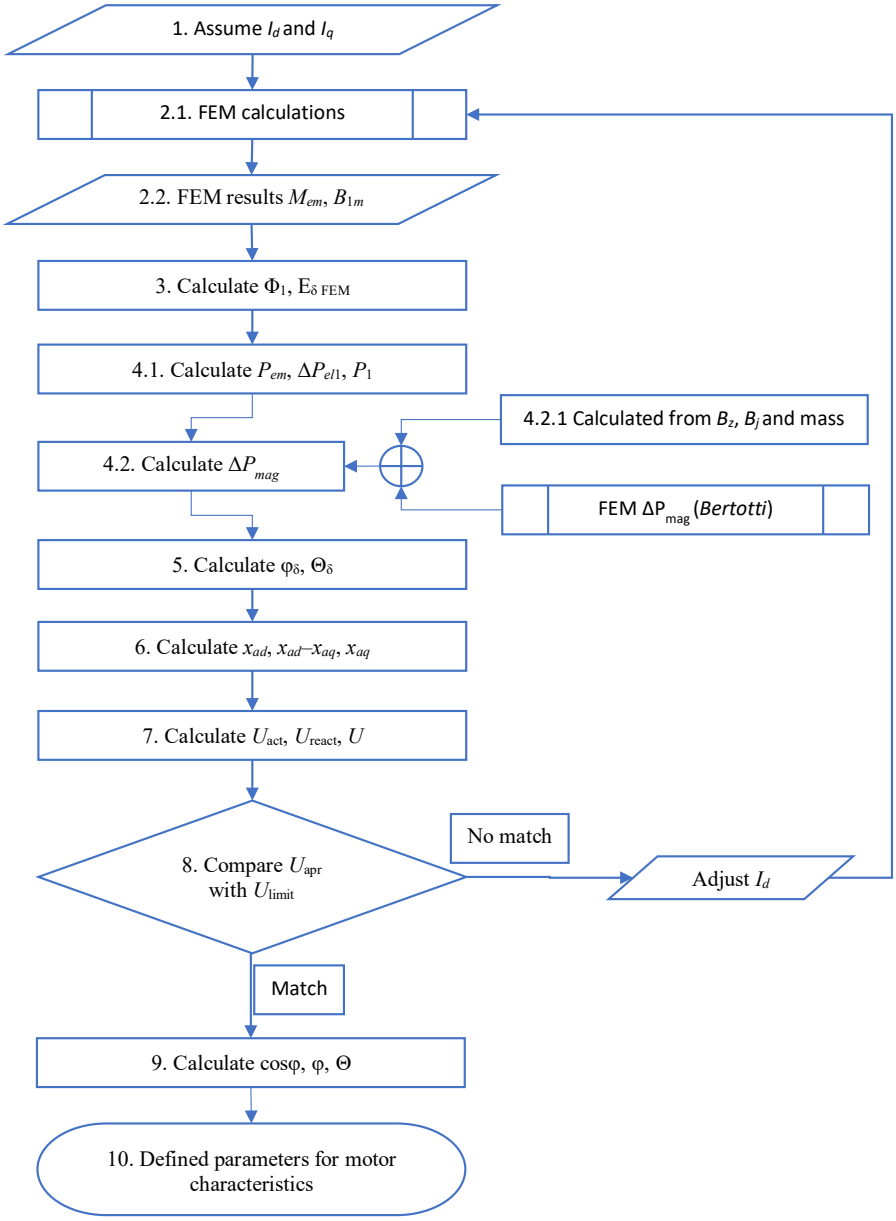

Fig. 2.14. Sequence of steps in the algorithm for calculating characteristic curves.

2.8. Finite element method in design

The numerical method for the calculation of electromagnetic fields, the finite element method (FEM), is widely used in the design of SynRMs, in the framework of this work and in the design of advanced electrical machines in general. A description in Latvian of the application of advanced FEM software in electrical engineering can be found in [27]. The FEM software *Flux* is used in the framework of this work, and its functionality and principle of operation do not differ significantly from other FEM software popular in industry and academia, such as *ANSYS*, *COMSOL* or *SolidWorks*. The application of *Flux* FEM software for modelling the magnetic field of an electrical machine is described in [28].

The SynRM FEM model is shown in Fig. 2.15:

1. Three-phase two-layer winding specified with slot current [A]. When the phase currents are specified, the position of the magnetic field with respect to the rotor position is determined, and consequently, the load angle Θ is defined.
2. Rotor and stator steel whose magnetic properties are given by the B(H) curve. For the calculation of magnetic losses, the specific loss versus induction and the thickness of the steel sheets are defined.
3. Non-magnetic air barriers on the SynRM rotor and the air gap between the stator and rotor are set to relative magnetic permeability $\mu_r = 1$.
4. The shaft and other magnetically and electrically inactive elements are assigned a material-specific relative magnetic permeability.
5. Finite element mesh of triangular elements. The network is made finer at geometric nodal points, such as the air gap.
6. The limit of the finite element model beyond which the magnetic field does not continue.

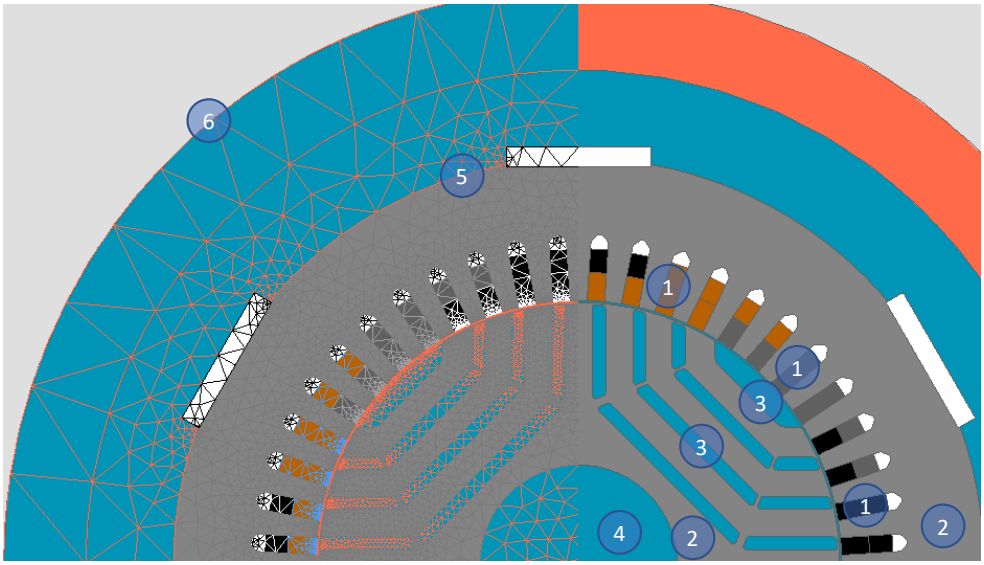

Fig. 2.15. SynRM FEM model with finite element mesh.

3. SYNCHRONOUS RELUCTANCE MACHINE COOLING SYSTEM FOR ENCLOSED DESIGN

3.1. SynRM cooling systems

In electrical machines, the design of the cooling system is as important as the electromagnetic design of the machine in determining the maximum power transfer, reliability, stability and longevity of the electrical machine. The selection of the optimum cooling system is particularly important in transport applications, where the external dimensions and weight of the electrical machine are limited. For most electrical machines, sufficient cooling is provided by air convection or the radiation of heat from the machine body to the surrounding environment, and heat dissipation through the machine mounts and shaft. A cooling system is passive if the heat is dissipated without additional energy consumption, only by convection and transfer to the mounts. Active cooling methods are used for electrical machines with high power densities. Fans are mainly used to create airflow or to promote heat transfer by the circulation of the coolant. The coolant transfers heat from the hottest parts of the machine, usually close to the winding, to the radiator.

3.2. SynRM thermal equivalent circuit

The equivalent scheme describing the SynRM heat transfer process is shown in Fig. 3.1, with the main simplification of considering the heat flow only in the radial direction. Several literature sources describe specifically the SynRM thermal equivalent scheme, where it is recommended to refer to references [29], [30], and [31] at the author's discretion.

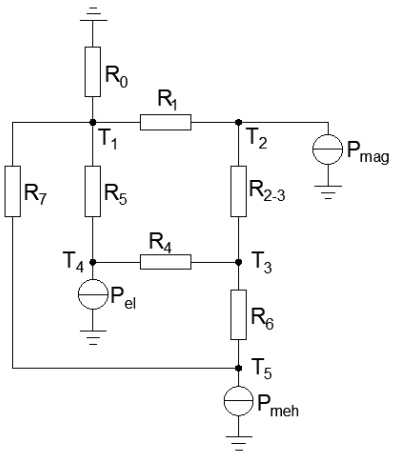

R_0 – ambient thermal conductive layer;
R_1 – heat conduction resistance of the upper part of the stator yoke;
R_{2-3} – the thermal conduction resistance of the inner part of the stator yoke and the stator tooth;
R_4 – heat conduction resistance between the stator slot and the stator;
R_5 – heat conduction resistance in the slot layers;
R_6 – convection resistance of the air gap;
R_7 – heat conduction resistance of the rotor.

Fig. 3.1. SynRM thermal equivalent schematic.

3.3. Heat loops cooling system

A liquid cooling system based on the change of state of the coolant, with natural circulation of the coolant in a closed loop, is called a heat loop. The term *heat pipe thermosyphon* (HL) is also used. The heat loop is based on the change of the aggregate state of the heat transfer medium in the evaporator from liquid to gas and in the vapour condenser from gas to liquid. A graphical interpretation of the operating principle of the heat loop is shown in Fig. 3.2. A heat loop is a closed-loop, passive, low-loss heat transfer system with no additional energy input for heat circulation.

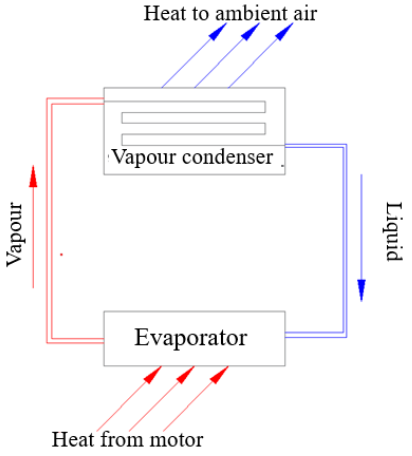

Fig. 3.2. Operating principle of a heat loop (HL).

The most technically complex element of a heat loop, in terms of design and manufacturing, is the evaporator. A graphical explanation of the heat loop cooling system is shown in Fig. 3.3, where:

1 – heat collector – evaporator unit with thermal interfaces to the machine, Fig. 3.3 b) shows the machine design with 12 evaporators;

2 – heat transfer channels (liquid and vapour line);

3 – cooling radiator – vapour condenser with air heat exchanger.

a) b)

Fig. 3.3. Heat loops cooling system: a) main elements of the heat loops; b) stator design with 12 evaporators.

3.4. Application of the finite element method in SynRM thermal modelling

The finite element method (FEM) has been employed in numerous scientific disciplines to address a wide range of complex physical problems. Its applications encompass domains such as solid mechanics, fluid and gas mechanics, electrical engineering, and a multitude of other technical fields. In Latvia, the utilisation of FEM has accumulated several decades of experience, encompassing not only the field of electrical engineering, a subject with which the author is intimately familiar, but also civil and mechanical engineering [32]. The primary benefit of the method is its capacity to mathematically model and numerically solve complex problems, a feature that has led to its extensive utilisation [33]. The author's expertise in FEM application primarily lies in the modelling of electromagnetic processes. However, beyond the studies outlined in this chapter, two notable studies [34], [35] that investigated, compared and described the application of FEM in SynRM thermal modelling, for which the author provided consultancy, are particularly noteworthy.

Example of FEM application in SynRM temperature modelling

The application of FEM to temperature modelling of a 180 kW SynRM with an IC01 cooling system presented in [36] is reviewed.

The FEM simulation results agree well with the experimentally determined results described in the next chapter of this Thesis, with the experimentally obtained winding temperature increasing from 17.7 °C to 88.6 °C, or by **70.9 °C,** during 60 min at rated load. The FEM results are shown in Fig. 3.4, where a) shows the steady-state temperature distribution obtained by modelling the thermodynamics problem for steady-state operation, and b) shows the temperature change in the stator tooth over 60 min obtained by modelling the transient thermodynamics problem; in nominal load mode, the temperature in the winding increases from 0 °C to 72 °C, or by **72 °C**, over 60 min.

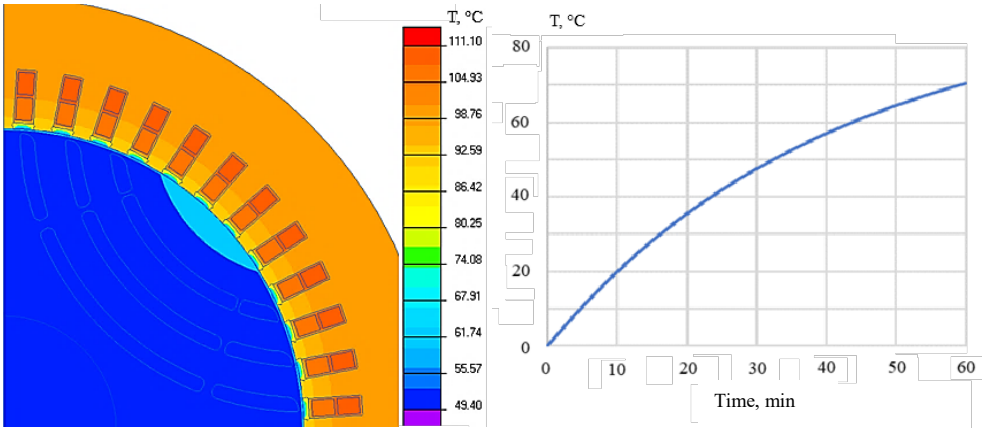

a) b)

Fig. 3.4. FEM simulation results for 180 kW SynRM: a) temperature distribution in the machine, steady state; b) temperature variation in the stator slot or winding with operating time, summary of FEM results.

Example of FEM application in SynRM with HL temperature modelling

The application of FEM to temperature modelling in SynRM with HL cooling presented in [37] is reviewed. The FEM modelling without HL is performed by setting the heat transfer coefficient on all external surfaces of the stator segment to $h = 4$ W/m^2/K (Fig. 3.5 a)). FEM modelling with HL is performed by setting the heat transfer coefficient on the external surfaces of the stator segment facing the adjacent segments and the rotor to $h_1 = 44$ W/m^2/K and for the surfaces facing the HL, to $h_2 = 44$ W/m^2/K (Fig. 3.5 b)).

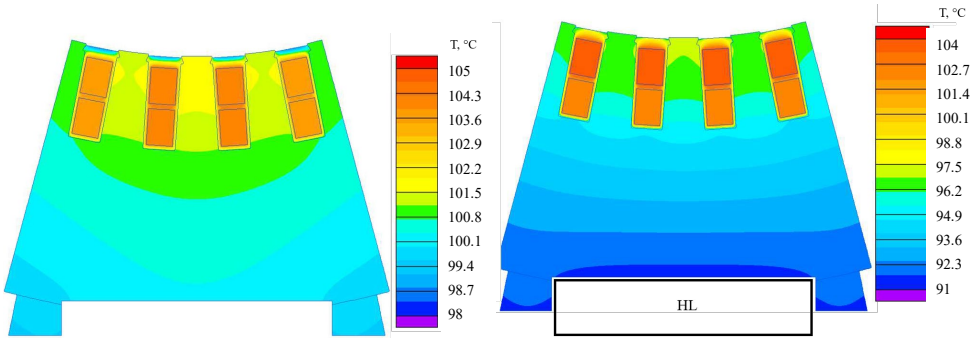

a) b)

Fig. 3.5. FEM simulation results for the SynRM segment:
a) without HL ($h = 4$ W/m^2/K); b) with HL (at HL $h = 44$ W/m^2/K).

Example of FEM application in temperature modelling of SynRM with cooling channels in slots

The FEM is used to simulate the temperatures of a 1/12 segment for which additional cooling channels are created in the stator slots, hereafter HL2. As before, a heat transfer coefficient $h_1 = 4$ W/m^2/K is assigned to all external surfaces of the segment. First, consider the variant where the channels are formed in the slots but no HL2 evaporators are inserted, with the air in the channels, respectively $h_2 = 4$ W/m^2/K, on the HL2 surface (Fig. 3.6 a)). The other option considered is with HL2 evaporators in the ducts, respectively $h_2 = 28$ W/m^2/K is specified on the HL2 surface (Fig. 3.6 b)).

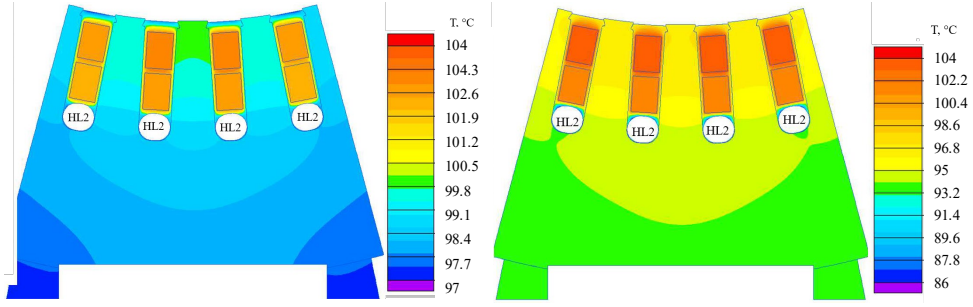

a) b)

Fig. 3.6. FEM simulation results for a SynRM segment with HL2 in the stator slots:
a) HL2 replaced by air ($h_2 = 4$ W/m^2/K); b) HL2 (at HL $h_2 = 28$ W/m^2/K).

4. SYNCHRONOUS RELUCTANCE MACHINE DEVELOPMENT

4.1. 180 kW SynRM

4.1.1. Design

Main dimensions

The 180 kW SynRM has been developed with the main project objective of replacing the 92.6 % efficient induction motor of a mass transit electric vehicle – a trolleybus – with a higher efficiency 95 % electric motor. The solution shall have the same external dimensions and power supply requirements as the induction motor to be replaced, as the solution is applied to an off-the-shelf vehicle with space constraints for the electric motor. Optimisation at the design stage is prioritised to maximise efficiency. It should be noted that the SynRM and its control system have been developed separately by designing the motor according to the main parameters given in Table 4.1 and then adapting the control system. A description of the SynRM-adapted control method and system is given in [3], [38], and [39].

Table 4.1

Key Requirements for the Development of SynRM

D_{as}	493	mm	Stator outer diameter
L	290	mm	Stator active length
D_v	60	mm	Shaft diameter
δ	1.2	mm	Air gap width
V_{N1}	420	V	Rated mains line voltage
f_1	50	Hz	Rated network frequency
m	3		Number of phases
P_N	180	kW	Rated mechanical power
T_N	1146	N*m	Rated mechanical torque
n_1	1500	min^{-1}	Nominal rotation speed
η	95 %		Motor efficiency to be achieved in the project
	S2 60 min		Operating mode according to IEC 60034-1:2022

SynRM stator

The stator dimensioning is similar to other AC machines, with the addition of finite element optimisation (FEA).

SynRM rotor

The number of rotor air barriers shall be $N_r = N_s \pm 2 \times 2p$, which ensures the least fluctuation of the torque. A rotor with $N_r = N_s - 2 \times 2p = 40$ is designed, as this rotor is simpler with fewer air barriers. A rotor with $N_r = 56$ is more difficult to manufacture.

The flux channels are about twice as wide as the air barriers. A ratio between 2 and 3 provides an optimum magnetic asymmetry x_d/x_q.

The choice of rotor air barrier shape is based on [38]. The air barriers are formed as a circle, and all air barriers have a fixed centre of the circle.

The shape of the rotor air barrier includes mechanical strength joints that form a path for the q-axis flux, but are necessary to ensure the mechanical strength of the rotor.

The rounding of the rotor air barriers at the air gap is made with a radius of 7 mm. This radius is optimum and compared to a 4 mm rounding, the torque ripple T_{ripple} is 2 % smaller.

Design results and magnetic field

The results of the calculations are compared with the experimental results in the graphs in Figs. 4.6–4.8. The magnetic field scenes modelled by the FEM for the nominal load mode are shown in Fig. 4.1 and for the no-load mode in Fig. 4.2.

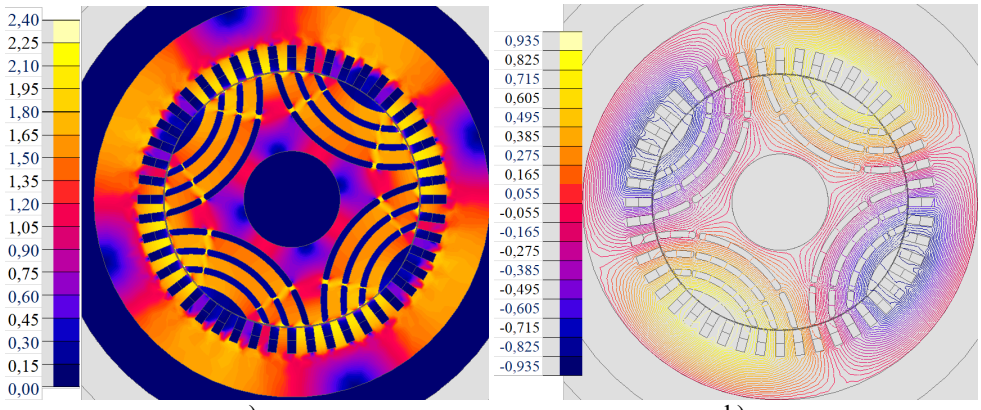

a) b)

Fig. 4.1. Magnetic field in nominal mode: I = 392 A, I_d = 125 A, I_q = 372 A; Θ = 29.9º:
a) magnetic flux density (T); b) vector potential (Wb/m).

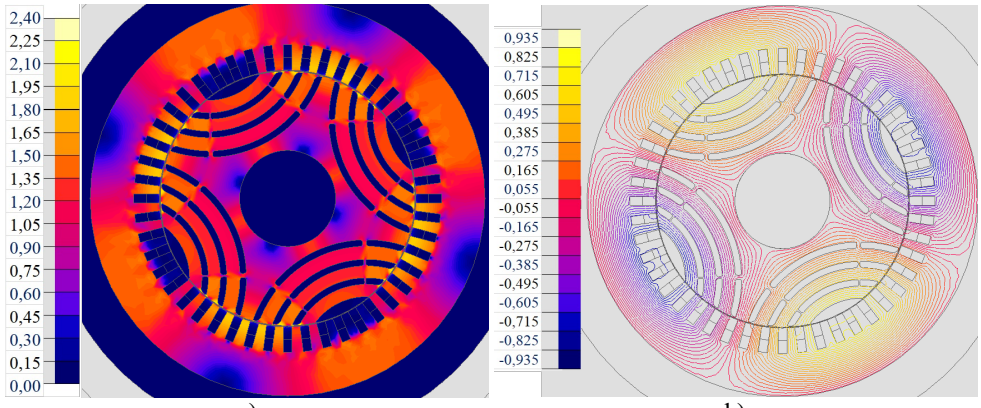

a) b)

Fig. 4.2. Magnetic field at no load: I = 126 A, I_d = 126 A, I_q = 0; Θ = 0:
a) magnetic flux density (T); b) vector potential (Wb/m)

The magnetic flux density in the air gap can be used to evaluate the electromagnetic torque ripple characteristic of the machine to be designed, as shown in Fig. 4.3. The magnetic flux

density curve shows the influence of the stator slots and the rotor air barriers on the electromagnetic torque ripple, highlighting that the designed machine has 48 stator slots and two pole pairs, while the magnetic flux density in the air gap has the most pronounced 23 and 25 harmonics since there are 48/2 = 24 slots per pole pair.

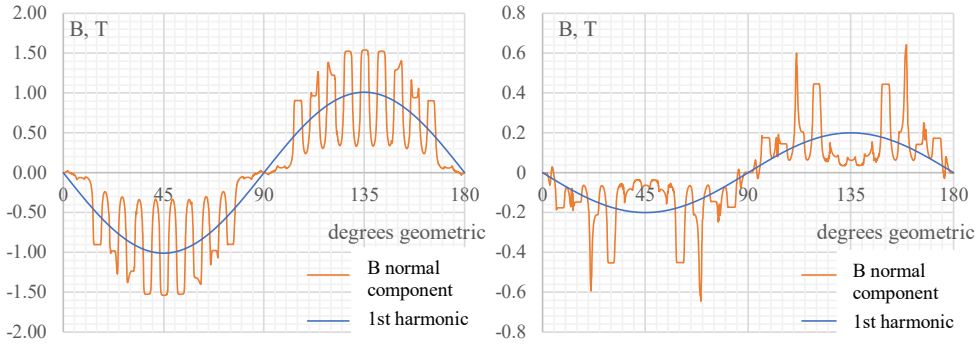

a) b)

Fig. 4.3. Magnetic flux density in the air gap at no load, normal component: a) d-axis (d); b) q-axis (q).

4.1.2. 180 kW SynRM experiments

Manufacturing

JSC "RER" produced the 180 kW SynRM prototype, largely using the company's well-honed induction machine technology. The similarity of the SynRM manufacturing process to that of an induction motor is considered to be a major advantage compared to that of permanent magnet motors.

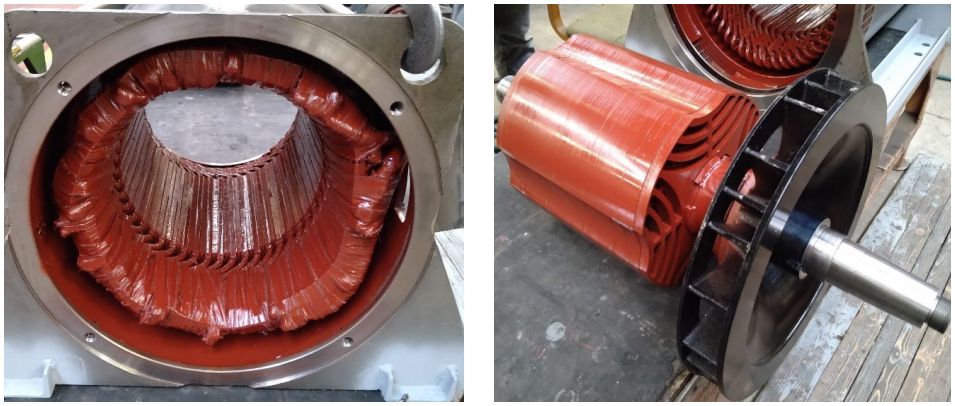

a) b)

Fig. 4.4. 180 kW SynRM manufactured by JSC "RER": a) stator; b) rotor.

Experiments

The 180 kW SynRM was tested in the laboratory of JSC "RER" on a special high-power transport electric motor test stand (Fig. 4.5). The laboratory bench used for the experiments and the experiment procedure are described in more detail in [3] and [39].

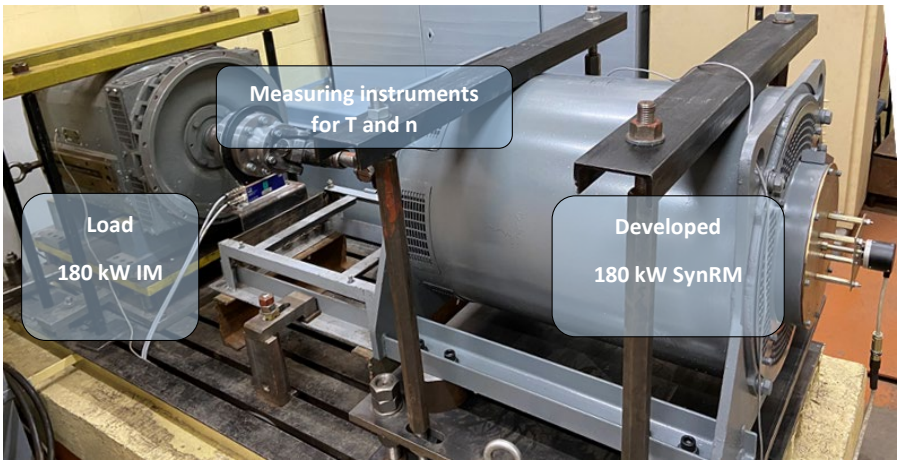

Fig. 4.5. 180 kW SynRM test stand.

Experiment results

The experiment results of the developed motor are summarised in Table 4.2 (Exp.); the electrical parameters are shown in Fig. 4.6, the torque in Fig. 4.7, the temperature and torque ripple in Fig. 4.8. The experimental results are presented in publications [20] and [38]. The experimental results are presented together with the parameters calculated at the design stage (Proj.), which were obtained using the calculation method presented in the previous chapter of this Thesis and in the publication [25].

Table 4.2

Results of the 180 kW SynRM Project and Experiment compared to induction motor (IM)

Parameters			**Proj.**	**Exp.**	**IM**
Stator current	I_1	A	392	374	310
Stator voltage	V_1	V	420	417	420
Power factor	cosφ	–	0.7	0.7	0.89
Electric power	P_1	kW	189	189	201
Mechanical power	P_2	kW	179	179	186
Mechanical torque	T_2	Nm	1141	1144	1193
Stator winding resistance	R_1	Ω	0.0122	0.0103	–
Stator electrical losses	$\Delta P_{el1\,N}$	kW	5.64	4.90	6.74
Rotor electrical losses	$\Delta P_{el2\,N}$	kW	–	–	2.17
Magnetic losses	ΔP_{mag}	kW	2.87	2.85	3.68
Mechanical losses	ΔP_{moss}	kW	0.54	0.82	0.47
Additional losses	ΔP_{add}	kW	1.00	0.86	1.03
Total losses	ΔP_{Σ}	kW	10.1	9.43	14.1
Efficiency ratio	η	%	94.7 %	95.0 %	92.5 %

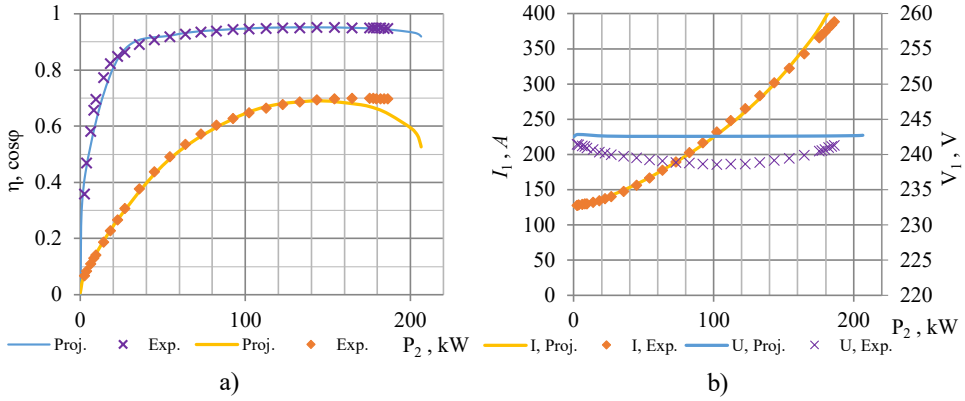

Fig. 4.6. 180 kW SynRM experimental and calculated performance curves: a) efficiency and power factors; b) voltage and current.

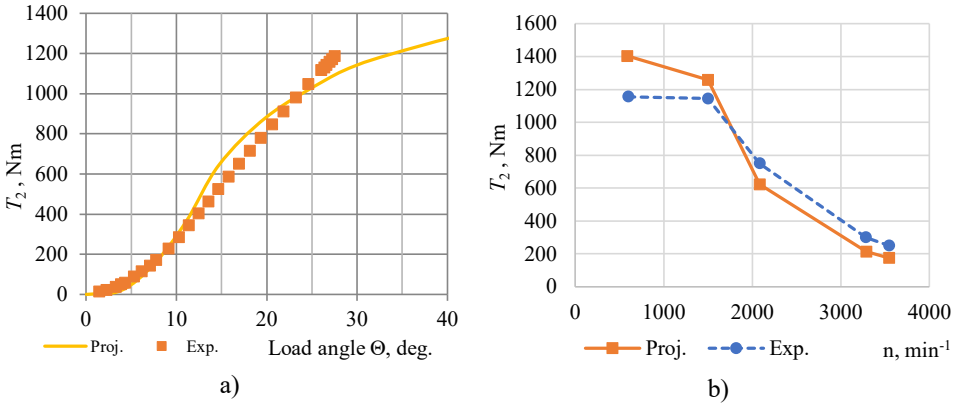

Fig. 4.7. 180 kW SynRM experimental and calculated performance curves: a) static, angle characteristic; b) traction characteristic.

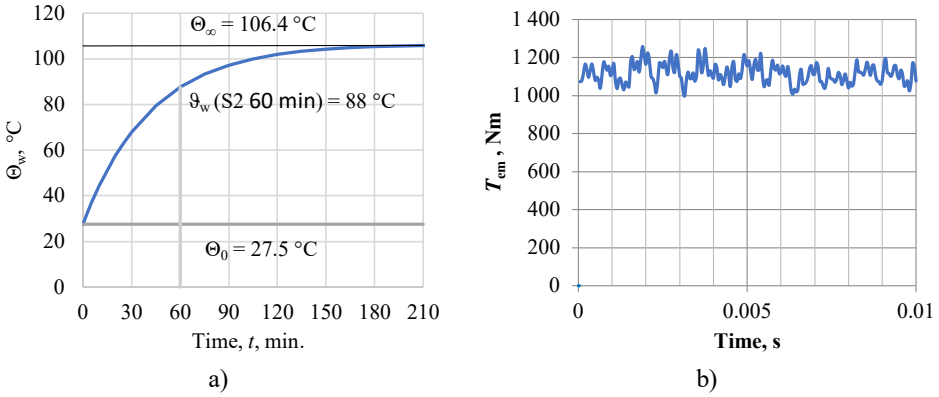

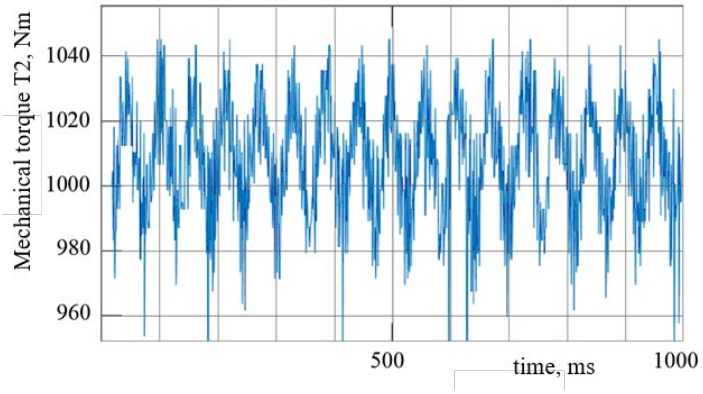

c)

Fig. 4.8. 180 kW SynRM experimental and calculated curves: a) stator winding temperature Θ_w; b) electromagnetic torque ripple, instantaneous value from FEM calculations; c) mechanical torque ripple, from experimental results.

4.2. Increasing the specific power of the SynRM with a heat-loop cooling system

The maximum power converted by an electric motor will be affected by both the design of the electromagnetic system and the ability of the cooling system to remove heat from the windings. By improving the performance of the cooling system of the electrical machine, either result can be achieved:

- increase the maximum power of the motor without increasing the winding temperature or reducing the thermal stability and reliability of the equipment;
- reduce electrical losses and the longevity of the motor by reducing winding temperatures.

In the framework of this Thesis, a solution is considered for an electromagnetic design of the SynRM that improves the performance of the cooling system, thus resulting in a machine with higher specific power [40].

4.3. Experimental investigation of a SynRM with HL 1/12 stator segment

In order to test the possibility of improving the SynRM parameters – specific power with the help of the HL cooling system, a 180 kW SynRM 1/12 stator segment was manufactured at the JSC "RER" electrical machine plant. The HL cooling system, manufactured by "Allatherm" Ltd, is attached to the stator segment. The stator segment connected to the HL cooling system segment is shown in Fig. 4.9, which shows the numbered components of the experiment bench. HL cooling system evaporator is shown in Fig. 4.10; the fragment includes 1/12 of the evaporators and vapour condensers of the complete machine.

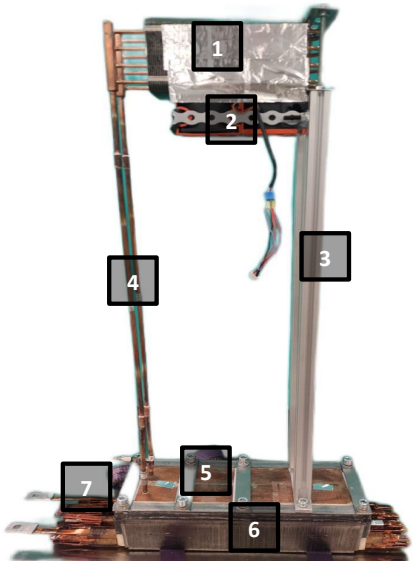

1 – vapour condenser

2 – fan

3 – fastening

4 – coolant fluid and vapour ducts

5 – evaporator

6 – stator fragment

7 – stator winding

Fig.e 4.9. Stator segment with HL cooling.

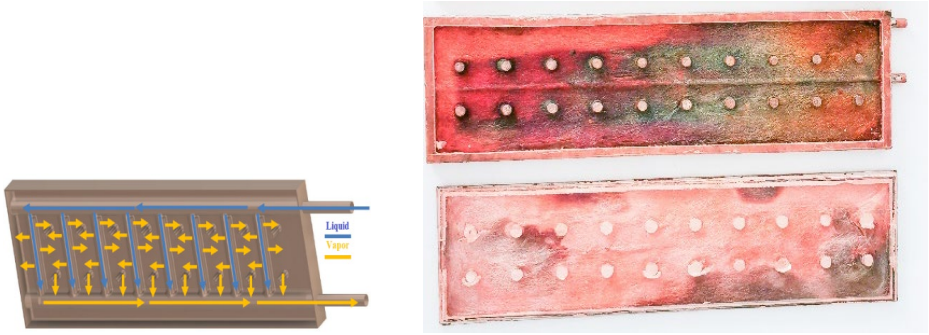

a) b)

Fig. 4.10. HL evaporator: a) schematic representation; b) fabricated capillary effect evaporator with wick-shaped copper parts.

Segment experiment results

The results of the segment experiment at a power output which produces a settled temperature in the stator windings equal to the 180 kW SynRM settling temperature $T°$ = 105 °C are shown in Table 4.3. The results are shown for one thermosensor per group, as there is only a minor difference in the measurement results within a group. From the experimental results, it can be observed that by using HL cooling, $\Delta P_{Cu\ (HL)}/\Delta P_{Cu\ (no\ HL)}$ = 350/138 = 2.54 times more power can be injected into the machine windings to maintain a constant winding temperature ~ $T°$ = 105 °C. The power ratio will depend on the load and the temperature, as shown in Fig. 4.11.

Table 4.3

Segment Experiment Results

Thermosensors / Segment cooling	Winding (No. 1)	Stator tooth (No. 4)	Stator surface (frame) (No. 13)	Power
	Temperature, T °C			W
Without HL	102	97	96	138
With HL	103	75	49	350

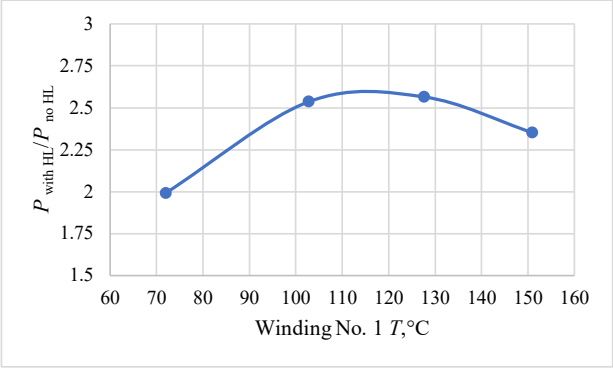

Fig. 4.11. Ratio of power applied to segment windings with and without HL cooling at steady-state temperature.

Segment experiment results applied to the full machine

The results of the segment experiment are summarised in Table 4.4.

Table 4.4

Comparison Between SynRM with HL and IC01 cooling

Parameters		Unit	SynRM with IC01 cooling	HL-cooled SynRM with reduced L	HL-cooled SynRM with increased P_2
Mechanical power	P_2	kW	**179.6**	**182.6**	**290.4**
Current	I	A	374	591	591
Electromagnetic torque	T_{em}	Nm	1144	1173	1980
Active length	L	mm	**290**	**168**	**290**
Stator outer diameter	D_{sa}	mm	493	493	493
Cu + Fe weight	$m_{Cu} + m_{(Fe)}$	kg	479	277	479
Power density		kW/kg	**0.37**	**0.66**	**0.61**
Electrical losses	ΔP_{Cu}	kW	4.9	11.5	14.3
Magnetic flux density in a tooth	B_z	T	2.05	2.16	2.16
Magnetic flux density in the yoke	B_j	T	1.72	1.93	1.93
Magnetic (iron) losses	ΔP_{Fe}	kW	2.9	2.4	4.2
Efficiency ratio	η	%	**94.9 %**	**92.2 %**	**93.4 %**

4.4. Experimental study of SynRM with HL in stator slots for 1/12 stator segment

Considering that for the above model, there is a significant difference between the winding temperature and the stator steel surface temperature when the HL machine is cooled, a design model was developed in which the HL cooling elements are located near the winding, hereafter referred to as Segment 2. Segment 2 was developed to investigate whether the heat dissipation efficiency can be improved by placing the cooling elements as close as possible to the main heat source, the winding.

The model produced for Segment 2 is shown in Fig. 4.12. When comparing the manufacturing process of the first segment with that of Segment 2, the disadvantage of Segment 2 is that during the manufacturing stage between the stator package and the winding in the slots, the cooling system elements have to be inserted into the slots. In the project for which the segment was produced, the responsibilities were divided: JSC "RER" was responsible for the production part of the electrical machine and "Allatherm" Ltd was responsible for the production of the cooling system, which reflects the production process of a typical electrical machine, in which the production of these parts will be carried out by separate departments or companies. The manufacturing process of *stator* > *winding* > *cooling* > *frame* is replaced by *stator* > *cooling* > *winding* > *cooling* > *frame*.

Due to manufacturing problems with the evaporator, the segment could not be tested, which demonstrates a major drawback of the solution: manufacturing complexity. The performance of the segment can be judged from the FEM modelling described in the previous section.

4.5. Experimental investigation of a full-scale SynRM with HL

SynRM 1/12 segment tests show the potential to cool SynRM with an HL cooling system. Applying the segment test results to the full machine with a number of simplifications, it can be concluded that the HL cooling system can not only cool the machine at the existing level but even increase the power density. However, the segment only partially describes the heat transfer process of the full machine. The application of the segment test to an enclosed machine has to be evaluated analytically, but it involves a number of assumptions, the most important of which are the influence of the fully closed design and the rotor rotational motion on the heat transfer process. A complete SynRM with HL cooling system has been built with the main objective to experimentally test the feasibility of a fully enclosed SynRM maintaining a power of 180 kW without increasing the external dimensions of the machine and without compromising the efficiency as much as possible (loss of about 2 %). Incorporation of HL into the SynRM design is shown in Fig. 4.19.

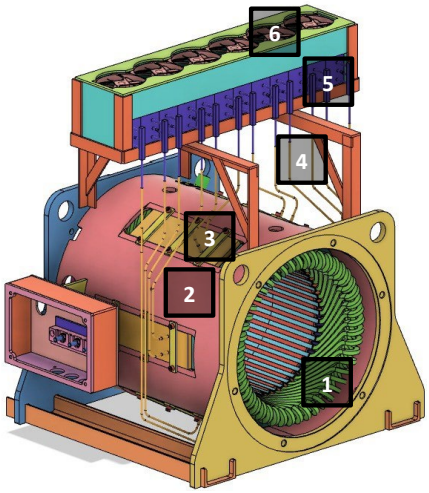

1 – SynRM stator with windings
2 – SynRM frame with openings for HL evaporator
3 – HL evaporator
4 – HL coolant fluid and vapour ducts
5 – HL vapour condensers
6 – HL fans

Fig. 4.19. Sketch of the HL-cooled SynRM.

The IC code (*International Cooling*) of the cooling system of the developed 180 kW SynRM with HL cooling system according to **IEC 60034-6:1991** is IC9W7.

Design

The design of the synchronous reluctance machine followed the guidelines described in the previous chapters. In order not to repeat what has been presented in the previous chapters, only the main differences of the SynRM with heat-loop cooling (hereafter referred to as the SynRM with HL) from the 180 kW SynRM with IC01 cooling (hereafter referred to as the 180 kW SynRM) are presented here. The SynRM with HL shall be similar to the 180 kW SynRM, with the aim of evaluating the cooling efficiency of the HL by comparing almost identical electrical machines whose main difference is the cooling system, HL or IC01, respectively.

The developed SynRM is designed with trapezoidal rotor air barriers (Fig. 4.14). The trapezoidal barriers have the disadvantage of achieving a lower electromagnetic torque compared to arc-shaped barriers, but the advantage is that the barrier edges are straight, which makes them easier to prepare and easier to insert permanent magnets into. The project does not consider increasing the power of the SynRM with permanent magnets, but the decision to use trapezoidal barriers was taken so that the prototype could be used in potential future PMASynRM studies.

The developed SynRM is designed with six HL evaporators. The evaporators partly occupy the space typically allocated to the clearance between the casing and the stator pack in order to have the least possible effect on the stator yoke height.

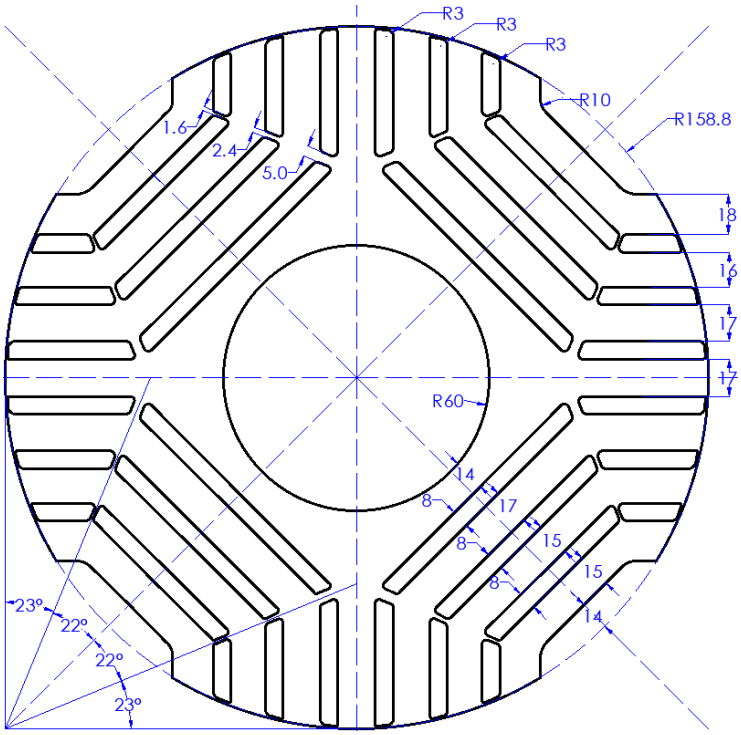

Fig. 4.14. SynRM with HL cooling, trapezoidal air barrier rotor.

Manufacturing

SynRM with HL manufactured by JSC "RER" is shown in Fig. 4.15. The stator (2) and rotor (1) of the machine are made of 0.5 mm-thick M470-50HP electrical steel sheets, shown in Fig. 4.15 a)). A rotor core is assembled on the shaft (3) from rotor electrical steel sheets (1), which are secured with an end fitting (4); then the core is laminated, shown in Fig. 4.15 b)). The assembly of the stator core begins with the manufacture of the frame cylinder part (5) to which the end plates (6) are welded. The stator electrical steel sheets (2) are inserted into the frame cylinder, shown in Fig. 4.15 c)), after which the slots of the assembled stator core are machined. In the next step, the active parts of the windings and the slot insulation are inserted into the slots. The front parts of the winding are connected according to the winding diagram and insulated. The assembled stator with windings is impregnated with an epoxy layer. The winding is 8.5 × 17 mm copper wire with a wire insulation thickness of 0.23 mm. The insulation of the slot is 0.9 mm to 1,75 mm thick. The insulation of the winding and the slot shall be of thermal resistance class (H) with a maximum permissible long-term temperature of 180 °C according to IEC 60085:2007. The stator and frame are painted. The manufacturing processes of the SynRM and the HL cooling system were separated. Separate production is considered an advantage. Finally, the manufactured HL cooling system evaporator (11), water and vapour transmission lines (12) and vapour condenser (13) are attached to the SynRM (Fig. 4.15 d)). The components of the heat loops cooling system were manufactured by "Allatherm" Ltd.

Experiments

The SynRM with HL has been tested in the laboratory of JSC "RER" on the test bench for electric motors for transport drives (Fig. 4.16). Experiments were carried out for two modes: no load mode and nominal load, or $P_2 = 180$ kW mode. The no-load experiment is carried out for approximately 2 h 25 min. The load experiment is carried out for about 1 h immediately after the no-load experiment, without switching off the machine.

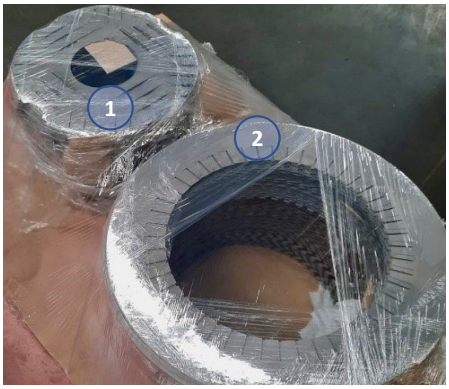

a)

b)

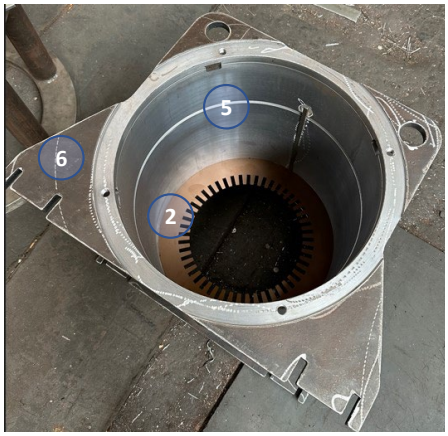

c)

d)

Fig. 4.15. Process for making SynRM with HL.

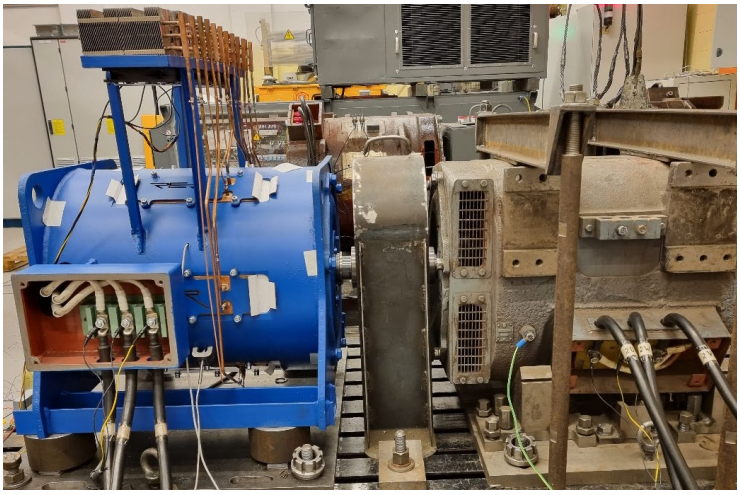

Fig. 4.16. SynRM with HL experimental bench.

Experiment results

Temperature measurements were taken for the heating (Fig. 4.17 a)) and cooling process (Fig. 4.17 b)). The heating process is divided into no-load (TG) and load (SL) modes. The cooling process is divided into the experiment with the HL steam condenser fan on (ROT) and with the HL steam condenser fan off (STAC). Temperature measurements were taken for a total of almost 24 h with temperature data *loggers* recording a measurement every ~ 10 s. The measured temperature in the slot directly at the winding, which is also the largest, the temperature on the machine surface (frame) and the ambient air temperature next to the experiment bench.

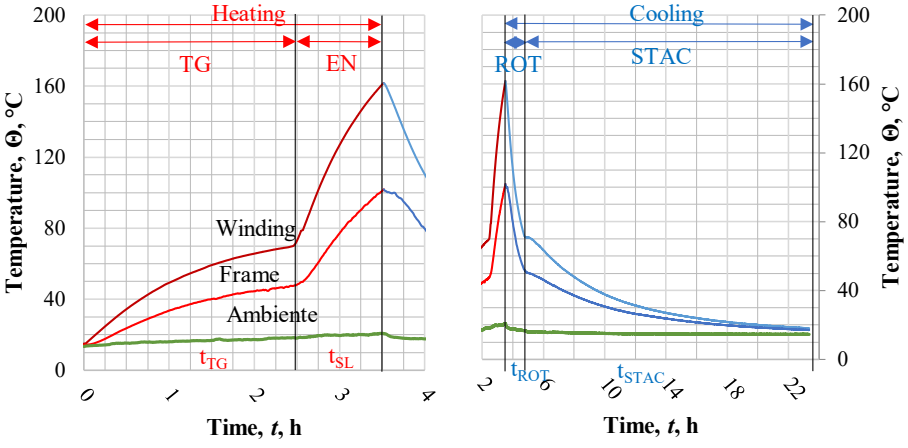

a) b)

Fig. 4.17. Results of the SynRM with HL experiment: a) heating at no load (TG) and nominal load (SL) modes; b) cooling with HL evaporator fans on (ROT) and HL evaporator fans off (STAC).

With some simplifications, the heating process of the SynRM with HL machine observed in the experiments and the temperature of the machine elements during the heating process Θ_{heat} can be described by Equation (4.1). The main simplification is that the equation does not include the first 5–10 min of the set mode, where the process of electrical mode changed, or load increase from no-load to load mode, or no-load speed-up takes place. The approximation does not take into account the ambient temperature, Θ_{amb} , changing during the experiment and, instead, uses the approximated starting temperature of the experiment – Θ_0. Interestingly, from the results of the experiment, a correlation can be observed in how the ambient temperature is affected by the heating process of the machine. The steady-state temperatures ϑ_∞ and the heating time constant T characteristic of the operating mode are an approximation of the experimental results. The experimental results (exp.) and the approximation (aprox.) using Equation (4.1) are shown graphically in Fig. 4.19. The temperatures, $\Theta_0, \vartheta_\infty$ and the heating time constant T for the different modes are summarised in Table 4.5 and explained graphically in Fig. 4.24.

$$\Theta_{\text{heat}} = \Theta_0 + \vartheta_\infty \left(1 - e^{\left(-\frac{t}{T}\right)}\right). \tag{4.1}$$

Using the heating time constants and stable over-temperatures obtained from the experimental results, it is possible to calculate the temperature of the HL-cooled SynRM at rated load $P_2 = 180$ kW after 60 min of operation time – S2 60 min at ambient temperature 40 °C, then $\Theta_w = 135$ °C and $\Theta_{\text{frame}} = 101$ °C for the HL-cooled SynRM.

The temperature of the elements in the cooling process, Θ_{cool}, can be described by Equation (4.2). The starting temperature, Θ_o, and the cooling time constant, T, are summarised in Table 4.5.

$$\Theta_{\text{cool}} = \Theta_{\text{amb}} + (\Theta_0 - \Theta_{\text{amb}}) e^{\left(-\frac{t}{T}\right)} \tag{4.2}$$

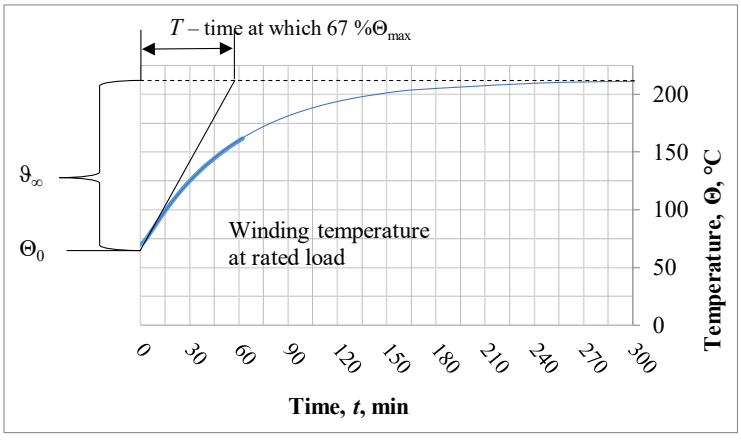

Fig. 4.18. SynRM with HL winding temperature $\Theta_0, \vartheta_\infty$ and heating time constant T.

Table 4.5

Temperatures Θ_0, ϑ_∞ and Heating Time Constant T

Mode / Measurement location / Parameter	Heating				Cooling			
	No load		**Load**		Rotation		Statistic	
	Winding	Frame	**Winding**	Frame	Winding	Frame	Winding	Frame
Temperature at the start of the experiment, **Θ_0, °C**	13	10	**65**	40	162	110	75	53
Stabilised surface temperature, **ϑ_∞, °C**	66	44.3	**147**	110	–	–	–	–
Heating time constant, ***T*, min**	75	80	**57.5**	75	75	80	300	320

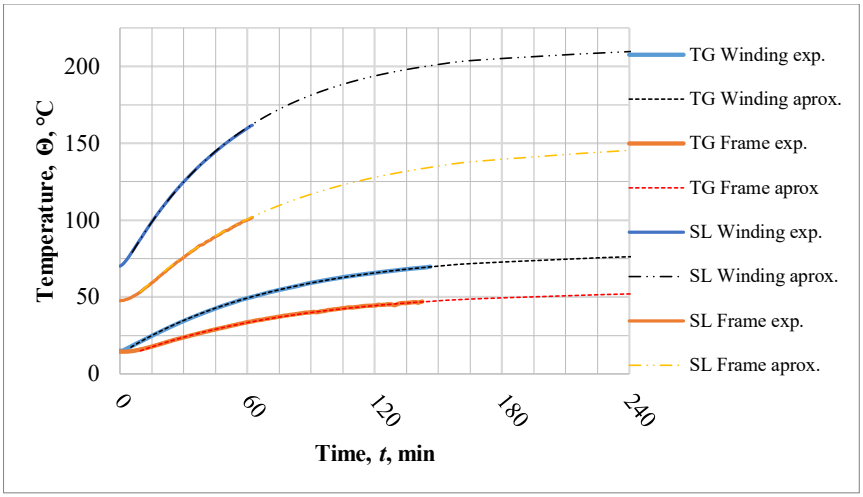

Fig. 4.19. SynRM with HL winding and case heating in no-load (TG) and load (SL) modes.

For the cooling experiment and the approximation of its results (Fig. 4.20 a)), the mode when the HL cooling system steam condenser fans (STAT) are switched off is particularly relevant. This cooling mode best describes a machine without a cooling system, which, according to EN 60034-6:2002 is designated as an IC00 cooling system, where the heat is transferred naturally from the enclosure to the ambient environment without a fan. By comparing the SynRM with the HL, SynRM IC00, SynRM IC01 heating time constants, and stable surface temperatures, the benefit of the HL cooling system can best be appreciated (Fig. 4.20 b)). It can be assumed with relatively high accuracy that under similar conditions, the cooling and heating time constants of the machine will be the same, which is confirmed by the data shown in Table 4.5 for the no-load heating experiment and the cooling experiment with the HL vapour condenser fans switched on. It should be noted that the time constant and steady state overtemperature for the IC00 closed loop machine will be higher than analytically determined, since the cooling experiment was performed in a SynRM with HL, the HL parts of which are made of copper, which has a better thermal conductivity compared to the steel of the IC00 machine casing.

The heating of the windings affects the active resistance of the winding, hence the electrical losses of the machine, so it is useful to evaluate the electrical losses of the SynRM with HL and compare them with the electrical losses of the SynRM IC01 (Fig. 4.20 c)). From the well-known resistance-temperature relationships, the effect of increased winding temperature on the active resistance of the winding and its corresponding electrical losses is analytically calculated. In nominal operation at P_{2N} = 180 kW, U = 420 V, f = 50 Hz, n = 1500 min^{-1}, the electrical losses of the SynRM with HL compared to the 180 kW SynRM with IC01 cooling are approximately ~ 0.5 kW higher, resulting in approximately ~ 0.3 reduction in efficiency.

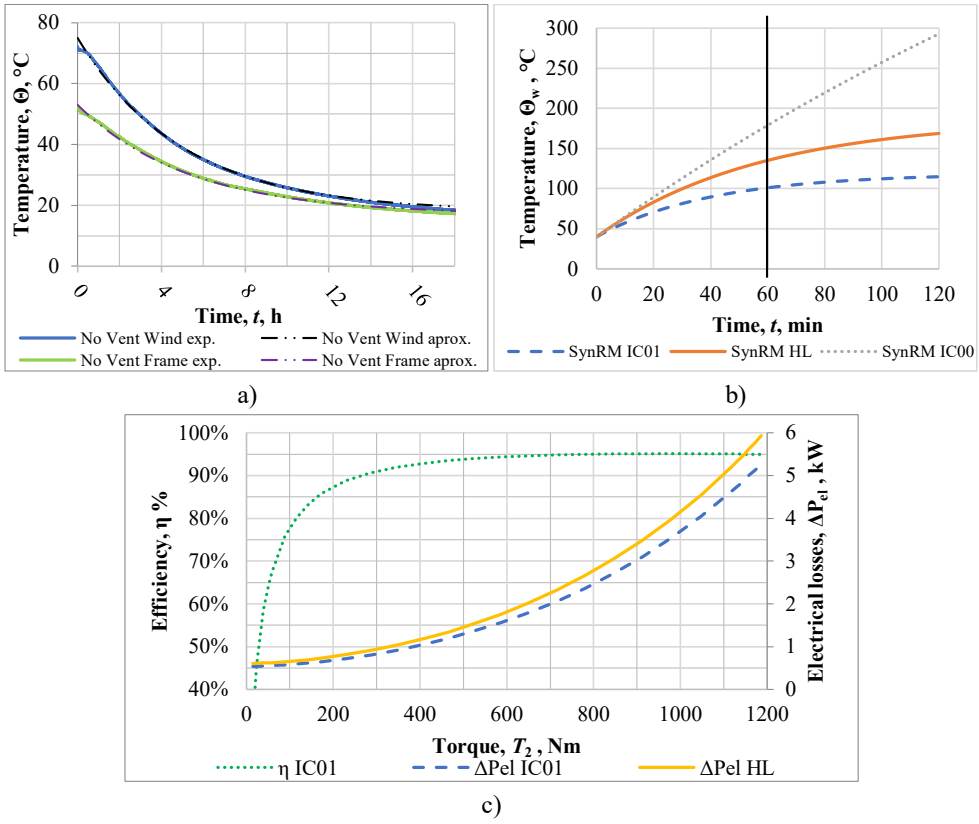

Fig. 4.20. a) SynRM with HL, winding (Wind) and frame (Frame) cooling experiment results (exp.) and calculated approximation (aprox.) with HL vapour condenser fans off (No Vent); b) SynRM with HL, SynRM IC01 and SynRM IC00 temperature comparison at ambient temperature, Θ_{amb} = 40 °C; c) Electrical losses of SynRM with HL and SynRM IC01 vs. load torque, at n = 1500 min^{-1}, U = 420 V, f = 50 Hz

For the SynRM with HL, the main experiments were temperature measurements; there were electrical measurements at no-load and nominal operation, which indicate the overall efficiency of the motor compared to the IC01 motor. The following measurements were taken in nominal load mode: U = 467.5 V; I_1 = 370 A; P_1 = 194.2 kW; cosφ = 0.648; f = 50 Hz; P_2 = 181.1 kW and consequently the efficiency is η = 93.3 %. Although the electrical losses have only

increased by 0.5 kW, compared to SynRM with IC01 cooling, the total losses have increased to $\Delta P_{\sum} = 13.1$ kW, an increase of 3.67 kW ($\Delta P_{\sum IC01} = 9.43$ kW).

During the experiment, infrared thermography is used to detect *hotspots*. The infrared thermography is taken with the same reflectance for the whole image. Infrared thermography images demonstrate the damaged HL evaporator. Figure 4.21 shows the thermal images at the end of the load experiment when the highest motor temperatures were reached.

The efficiency of the HL cooling system can be judged by the temperature ratio between the evaporator and the vapour condenser (Fig. 4.22). The higher the temperature ratio, the more efficient the cooling system. When the evaporator/vapour condenser temperature ratio is considered together with the system temperature, the higher the cooling temperature, the higher the efficiency of the HL cooling system (Fig. 4.22). Interestingly, there are some jumps in the efficiency of the HL cooling system, which may be due to the change in the aggregate state of the water in the HL evaporator.

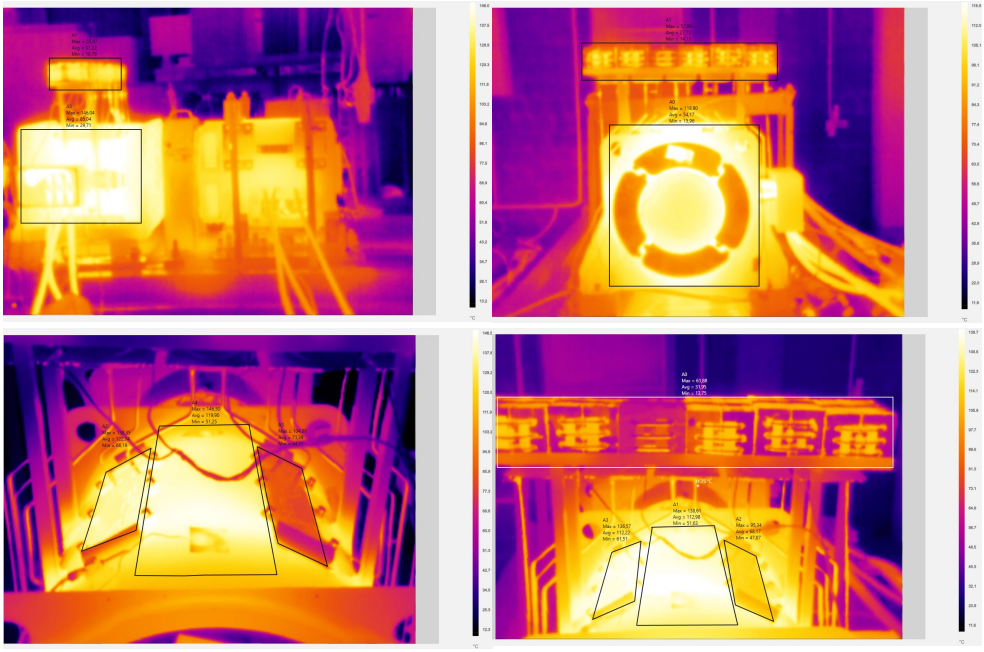

Fig. 4.21. Thermal images of the SynRM with HL before the cessation of the heating mode when the maximum motor temperatures are reached.

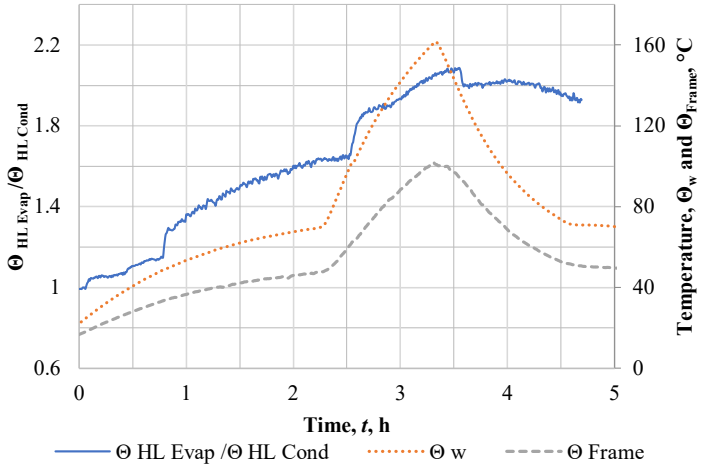

Fig. 4.22. Relationship of HL evaporator (HL Evap) and HL vapour condenser (HL Cond) temperatures on the same time scale with winding and frame temperatures.

MAIN RESULTS AND CONCLUSIONS

180 kW SynRM replacing the induction motor in a trolleybus

1. A 180 kW SynRM for public transport applications has been designed, manufactured and tested. The 180 kW SynRM is more efficient at rated load (n = 1500 min^{-1}; 180 kW), η_{SynRM} = 95 %, compared to the induction motor it replaces, η_{IM} = 92.5 %. The external dimensions and frame of the developed SynRM are the same as those of the induction motor it replaces. The induction motor is used in the trolleybus drive system currently manufactured by JSC "RER".

2. The parameters and characteristic curves of the SynRM have been calculated at the design stage using a developed calculation methodology, which has been validated by experimental results.

3. The experimental results show that the motor does not experience any significant torque ripple. The design of the SynRM rotor is based on a number of prerequisites, such as the number, position and width of the air barriers to limit the electromagnetic torque ripple and the resulting mechanical torque ripple.

4. The developed motor has been demonstrated to exhibit high efficiency, but low overload capability. The motor has been designed with the objective of obtaining maximum power at a given set of external dimensions, voltage and efficiency. For a given set of external dimensions and rotor design, the maximum torque can be increased by increasing the current. However, for safe operation, it is necessary to use a higher-performance cooling system.

5. The cooling of the developed 180 kW SynRM is achieved through an open casing design with forced air circulation, with the fan mounted on the motor shaft IC01. This design corresponds to the cooling system of the induction motor that is to be replaced. The steady-state temperature of the motor winding at the rated load is 107 °C. The SynRM exhibits lower losses compared to the induction motor it replaces, resulting in reduced winding temperature.

SynRM with heat-loops cooling and closed design

6. A heat-loop (HL) cooled SynRM has been developed and experimentally tested, which achieves the main objective of the work to develop a fully enclosed SynRM while maintaining the rated power of 180 kW, without increasing the external dimensions of the machine and without significantly (~ 1.7 %) degrading the efficiency, as long as the winding temperature in the rated operating mode S2 for 60 min does not exceed the maximum temperature of 180 °C permissible for insulation class H over a long time period.

7. In accordance with the criteria stipulated in IEC 60034-6:1991, the International Cooling (IC) code designated for the HL cooling system of the 180 kW SynRM is IC9W7.

8. The HL-cooled SynRM, with six HL evaporator and vapour condenser circuits, has inferior cooling conditions compared to the 180 kW SynRM with IC01 cooling. IC01 is

an open machine with a fan mounted on a motor shaft. As the SynRM is designed for an operating mode S2 of 60 min, it is useful to compare the winding temperatures of the machines in rated load mode $P_2 = 180$ kW, $n = 1500$ min^{-1} after an operating time of 60 min, at an ambient temperature of 40 °C, the SynRM IC01 $\Theta_w = 101$ °C and the SynRM with HL $\Theta_w = 135$ °C.

9. For the HL-cooled SynRM compared to the uncooled IC00, the heat transfer is by convection between the machine body and the ambient air. The HL-cooled SynRM has significantly better cooling conditions at rated load $P_2 = 180$ kW, $n = 1500$ min^{-1} after 60 min running time, analytically determined that at ambient temperature 40 °C, SynRM IC00 $\Theta_w = 179$ °C.

10. The full SynRM with HL machine is designed with six HL evaporator and vapour condenser circuits, but it is technically possible to install twice as many evaporators of the same size for a total of 12 HL evaporator and vapour condenser circuits. With 12 HL circuits, a greater cooling effect would be obtained, potentially reaching lower temperatures than the SynRM with IC01 cooling.

11. The developed HL cooling system functions without the utilisation of pumps for the forced circulation of coolant. The circulation of coolant (water) is accomplished by the transition of water from a liquid state to a vapour state, and vice versa, in accordance with the closed-loop thermosyphon principle. This is facilitated by the placement of vapour condensers above the machine. To enable the alteration of water's aggregate state in response to thermal stimuli, the evaporator must possess a particular porous configuration. Achieving this configuration constituted a significant challenge in the manufacturing process.

12. To facilitate the mass deployment of the heat loop cooling system, it is necessary to enhance the reliability and production quality of the evaporators. During the experiment, one evaporator failed completely, and the efficiency of another evaporator was reduced. It is hypothesised that if all six HL evaporators had been operational, the experimental results would have been more favourable and the winding temperature would have been 5 °C lower.

13. The installation of HL evaporators on a SynRM stator pack has been observed to result in a substantial temperature difference between the winding and the steel surface of the stator. The enhancement of the cooling system's efficiency and responsiveness can be achieved through the improvement of the heat exchange process between the windings and the HL. The heat transfer process can be enhanced by the following measures: 1) reducing the thermal insulation, which would impact the dielectric properties of the slot and winding insulation and is therefore undesirable; 2) bringing the HL cooling system closer to the winding, which is a potential subject for future research.

14. The integration of the heat-loop evaporator within the slots of the stator necessitates the incorporation of cooling system components during the manufacturing process, situated between the stator assembly and the insertion of the winding into the slot. This

augmentation of the manufacturing process contributes to the complexity of the machine assembly.

15. Infrared thermography was employed to ascertain the temperature distribution across the machine body, with the focus being on the area between the two HL evaporators. The results revealed the absence of any notable hotspots, with the exception of the non-functional HL evaporator. This finding suggests that the cooling system, comprising six circuits of HL evaporator and vapour condenser, is adequately thermally balanced.

16. In the context of the developed SynRM, the highest efficiency of the HL cooling system is observed to be 2, with efficiency defined as the ratio of the HL evaporator and HL vapour temperatures. This ratio has been shown to exceed 2 when the winding temperature exceeds $\Theta_w > 140$ °C. The experimental results demonstrate that the heat loop efficiency is enhanced at higher temperatures, a property that renders it particularly well-suited for transport applications where high power densities and high temperatures are prevalent.

17. The development of the SynRM with HL has resulted in a significant reduction in external dimensions when compared to the SynRM IC01, due to the absence of a fan mounted on the shaft. The 180 kW SynRM IC01 utilises a fan with an axial length of 125 mm, which corresponds to approximately 15 % of the total shaft length of 817 mm. It is important to note that the SynRM with HL is equipped with an additional vapour condenser in comparison to the SynRM IC01. The advantage of the HL vapour condenser is that it can be mounted in a location that is not as premium, or even on the roof of the vehicle, where the cooling conditions of the vapour condenser are significantly improved when the vehicle is in motion. During the winter heating season, the heat collected by the HL cooling system can potentially be utilised to heat the vehicle cabin.

Potential future research

18. Further research opportunities for SynRM include the insertion of permanent magnets into the rotor barriers, resulting in PMASynRM. PMASynRM exhibits several advantages over SynRM, including higher efficiency, power factor and power density. However, it also has several disadvantages, including the possibility of demagnetisation of the magnets and manufacturing difficulties with the insertion and fixing of the magnets.

19. Further research opportunities for SynRMs with a closed design include the investigation of a hybrid cooling system. The following potential hybrid cooling system is outlined in the Thesis: the motor casing is cooled by a heat pipe system, which is set up as described, and channels are created in the stator slots to allow forced circulation of the heat transfer medium by a pump. This configuration would leverage the passive cooling of the heat exchanger; however, under conditions of high load and when the temperature attains a specified threshold, an auxiliary cooling system is to be activated in proximity to the winding.

LIST OF REFERENCES

1. European Council. European Green Deal [online]. Accessed: 09.2024. Available: https://ec.europa.eu/commission/presscorner/detail/lv/ip_19_6691
2. Rare Earth Magnets and Motors: A European Call for Action. A report by the Rare Earth Magnets and Motors Cluster of the European Raw Materials Alliance. Berlin 2021. [online]. Accessed: 09.2024. Available: https://eit.europa.eu/sites/default/files/2021_09-24_ree_cluster_report2.pdf
3. Zarembo, J. Research and Development of the Synchronous Reluctance Motor Traction Drive. PhD Thesis. Riga: [RTU], 2022. 80 p.
4. Lipo, T. A. Synchronous Reluctance Machines – A Viable Alternative for AC Drives? In: Electrical Machines and Power Systems, 1991, pp. 659–671.
5. Kostko, J. K. Polyphase Reaction Synchronous Motor. In: Journal of the American Institute of Electrical Engineers, Vol. 42, No. 11, 1923.
6. Vagati, A. Synchronous Reluctance Electrical Motor Having A Low Tourque-Ripple Design, Publication number 5818140 A, Publication date Oct. 6, 1998.
7. Vagati, A., Pastorelli, M., Franceschini, G., Petrache, S. C. Design of Low-Tourque-Ripple Synchronous Reluctance Motors, IEEE Transactions on Industry Applications Vol. 34, No. 4, 1998.
8. Almeida, A. T., Ferreira, F. J. T. E., and Baoming, G. Beyond Induction Motors – Technology Trends to Move Up Efficiency. In: IEEE Transactions on Industry Applications, Vol. 50, No. 3, pp. 2103–2114, May–June 2014.
9. ABB is first to reach anticipated IE6 hyper-efficiency with magnet-free motors, ABB, Jun. 2024. [online] (Accessed 5.11.2024 – library.e.abb.com)
10. Lipo, T. A., Matsuo, T. Rotor design optimization of synchronous reluctance machine. IEEE Transactions on Energy Conversion, Vol. 9, No. 2, 1994.
11. Pyrhonen, J., Jokinen, T., Hrabovcova, V. Design of Rotating Electrical Machines, John Wiley & Sons, Ltd., 2008.
12. Boldea, I., Nasar, S. A. The Induction Machines Design Handbook, second eddition, CRC Press, 2009, 845 p.
13. Boldea, I., Reluctance Synchronous Machines and Drives, Oxford: Clarendon Press, 1996, 230 p.
14. Taghavi, S., and Pillay, P. A Sizing Methodology of the Synchronous Reluctance Motor for Traction Applications. In: IEEE Journal of Emerging and Selected Topics in Power Electronics, Vol. 2, No. 2, pp. 329–340, June 2014.

15. Bomela, X. B., Kamper, M. J. Effect of Stator Chording and Rotor Skewing on Performance of Reluctance Synchronous Machine. IEEE Transactions on Industry Applications, Vol. 38, No. 1, 2002.

16. Gulbis, K. Sinhronās reaktīvās mašīnas konstrukcijas izstrāde, Maģistra darbs, Rīgas tehniskā universitāte, Rīga, 2016. 105 p.

17. Wang, K., Zhu, Z. Q., Ombach, G., Koch, M., et al. Optimal Slot/Pole and Flux-Barrier Layer Number Combinations for Synchronous Reluctance Machines. In: IEEE Ecological Vehicles and Renewable Energies, Monte Carlo, 2013.

18. Haataja, J. A comparative performance study of four-pole induction motors and synchronous reluctance motors in variable speed drives, Lappeenranta University of Technology, 2003.

19. Hrabovcova, V., Rafajdus, P., Janousek, L., Hudak, P. Influence of axially laminated Rotor Arrangement on the Saliency Ratio of 4 Pole Reluctance Synchronous Motor. In: Workshop on Electrical Machines' Parameters, Technical University of Cluj-Napoca, 26 May 2001.

20. Kamoliņš, E., Gorobecs, M., Burenin, V., Gulbis, K., Potapovs, A., Brakanskis, U., Zarembo, J., Sējējs, K. 180 kW Synchronous Reluctance Motor for Mass Transit Electrical Traction Application. In: 2021 23rd European Conference on Power Electronics and Applications (EPE'21 ECCE Europe), Belgium, Ghent, 6–10 Sept. 2021.

21. Gulbis, K., Kamoliņš, E., Brakanskis, U. Synchronous Reluctance Machine with Improved Design of Rotor Mechanical Strength Connections. In: 2016 IEEE 4th Workshop on Advances in Information, Electronic and Electrical Engineering (AIEEE 2016): Proceedings, Lithuania, Vilnius, 10–12 Nov. 2016.

22. Gulbis, K. Sinhronās reaktīvās mašīnas konstrukcijas izstrāde, Maģistra darbs, Rīgas tehniskā universitāte, Rīga, 2016. 105 p.

23. Kolehmainen, J. “Synchronous reluctance motor with form blocked rotor,” IEEE Trans. Energy Convers., Vol. 25, No. 2, pp. 450–456, Jun. 2010.

24. Lendenmann, H., Osterholm, V. Synchronous Reluctance Machine Using Rotor Flux Barriers as Cooling Channels, Publication number: US20130099607 A1, Issue date: Apr. 25, 2013.

25. Gulbis, K., Kamoliņš, E., Brakanskis, U., Zarembo, J. Parameter Calculation Method of Synchronous Reluctance Motor Including Cross Magnetic Saturation. In: 2020 IEEE 61st International Scientific Conference on Power and Electrical Engineering of Riga Technical University (RTUCON), 5–7 Nov. 2020.

26. Kamper, M. J. Effect of rotor dimensions and cross magnetisation on Ld and Lq inductances of reluctance synchronous machine with cageless flux barrier rotor. In: IEEE Proceedings – Electric Power Applications, Vol. 141, No. 4, pp. 213–220, 1994.

27. Zviedris, A., Podgornovs, A. Divdimensionālu magnētisko lauku matemātiskā modelēšana ar galīgo elementu metodi, Programma *Quick Field*, instrukcija, Rīga, 2007, 59 p.

28. Gulbis, K., Ātrgaitas ventiļdzinējs ar ārēju, reaktīvu rotoru, Inženierprojekts, Rīgas tehniskā universitāte, Rīga, 2014, 112 p.

29. Ghahfarokhi, P. S., Kallaste, A., Vaiman, T., and Belachen, A. Thermal Analysis of Totally Enclosed Fan Cooled Synhronous Reluctance Motor-state of art. In: 45th Annual Conference of the IEEE Industrial Electronics Society, pp. 4372–4377, October 2019.

30. Ghahfarokhi, P. S., Kallaste, A., Podgornovs, A., Belahcen, A., Vaimann, T. Development of analytical thermal analysis tool for synchronous reluctance motors. In: IET Electric Power Applications, pp. 1828–1836, 5 August 2020.

31. Ghahfarokhi, P. S., Kallaste, A., Belahcen, A., Vaimann, T. "Hybrid Thermal model of synchronous reluctance machine," Case studies in Thermal Engineering, pp. 381–389, December 2018.

32. Rikards, R., Čate, A. Galīgo elementu metode, Rīga: Rīgas Tehniskā universitāte, 2001.

33. Bathe, K. "The finite element method," Massachusetts Institute of Technology, 2008.

34. Kunkulbergs, R. Termisko procesu izpēte elektriskajās mašīnās ar matemātiskām skaitliskajām metodēm, Maģistra darbs, Rīgas Tehniskā universitāte, Rīga, 2021. 90 p.

35. Lavrinoviča, L. Siltumslodzes sadalījums vilces reaktīvajam dzinējam ar jaudu 180 kW, Inženierprojekts, Rīgas Tehniskā universitāte, Rīga, 2022. 74 p.

36. Lavrinoviča, L., Podgornovs, A., Bižāns, A., Gulbis, K. Overview of Thermal Loads Distribution in Traction Electric Machines and Conditions for Forced Cooling of Their Parts. In: 2022 International Conference on Electrical, Computer and Energy Technologies (ICECET 2022), Czechia, Prague, 20–22, Jul., 2022.

37. Lavrinoviča, L., Gulbis, K., Podgornovs, A., Bižāns, A. Analysis of the Heat Dissipation of Synchronous Motor with Reluctance Rotor with Goal of Power Density Increasing. In: 2023 International Conference on Electrical Drives and Power Electronics (EDPE 2023): Proceedings, Slovakia, The High Tatras, 25–27, Sept., 2023.

38. Gulbis, K., Brakanskis, U., Kamoliņš, E., Gorobecs, M., Potapovs, A., Sējējs, K., Zarembo, J., Burenin, V. Analysis of Test Results of the Developed Synchronous Reluctance Motor for Public Transport Application. Latvian Journal of Physics and Technical Sciences, 2022, Vol. 59, No. 4, pp. 25–41.

39. Burenin, V., Zarembo, J., Žiravecka, A., Ribickis, L. Model of Laboratory Test Bench Setup for Testing Electrical Machines. In 2020 IEEE 61st International Scientific Conference on Power and Electrical Engineering of Riga Technical University (RTUCON), Riga, Latvia, 2020.

40. Gulbis, K., Podgornovs, A., Bižāns, A., Lavrinoviča, L. Increasing the Power Density of 180 kW Synchronous Reluctance Motor by Implementing Loop Heat Pipe Cooling. In: 2023 3rd International Conference on Electrical, Computer, Communications and Mechatronics Engineering (ICECCME 2023), Spain, Santa Cruz de Tenerife, 19–21 July, 2023. Piscataway: IEEE, 2023, pp. 1–5.

Kārlis Gulbis was born in 1989 in Aizpute, Latvia. He received a Bachelor's degree (2012), an Engineering Qualification (2014), and a Master's degree (2016) in Energy and Electrical Engineering from Riga Technical University. Since 2013, he has worked at Riga Technical University, where he is currently a lecturer and researcher. In addition to research and working with students, he has worked in the field of electricity supply management since 2016 and is currently a senior electrical engineer at "State Real Estate" SJSC.

His research interests are in the fields of electrical machines for transport, renewable energies and mathematical modelling of electrical machines.